The Astrophysical Journal, 698:1989–2013, 2009 June 20 doi:10.1088/0004-637X/698/2/1989
© 2009. The American Astronomical Society. All rights reserved. Printed in the U.S.A.

SPITZER/IRAC–MIPS SURVEY OF NGC 2451A AND B: DEBRIS DISKS AT 50–80 MILLION YEARS

Zoltan Balog[1,5], László L. Kiss[2], József Vinkó[3], G. H. Rieke[1], James Muzerolle[1], András Gáspár[1], Erick T. Young[1], and Nadya Gorlova[4]
[1] Steward Observatory, University of Arizona, 933 North Cherry Avenue, Tucson, AZ 85721, USA; zbalog@as.arizona.edu
[2] Sydney Institute for Astronomy, School of Physics A28, University of Sydney, NSW 2006, Australia
[3] Department of Optics and Quantum Electronics, University of Szeged, H-6720 Szeged, Hungary
[4] Department of Astronomy, University of Florida, Gainesville, FL 32611-2055, USA
Received 2009 January 16; accepted 2009 April 22; published 2009 June 5

ABSTRACT

We present a *Spitzer* IRAC and MIPS survey of NGC 2451A and B, two open clusters in the 50–80 Myr age range. We complement these data with extensive ground-based photometry and spectroscopy to identify the cluster members in the *Spitzer* survey field. We find only two members with 8 μm excesses. The incidence of excesses at 24 μm is much higher, i.e., 11 of 31 solar-like stars and 1 of 7 early-type (A) stars. This work nearly completes the debris disk surveys with *Spitzer* of clusters in the 30–130 Myr range. This range is of interest because it is when large planetesimal collisions may have still been relatively common (as indicated by the one that led to the formation of the Moon during this period of the evolution of the solar system). We review the full set of surveys and find that there are only three possible cases out of about 250 roughly solar-mass stars where very large excesses suggest that such collisions have occurred recently.

Key words: circumstellar matter – infrared: stars – open clusters and associations: individual (NGC 2451) – planetary systems: protoplanetary disks

Online-only material: color figures, machine-readable tables

1. INTRODUCTION

Studying the evolution of disks around young stars offers the opportunity to understand the formation of planetary systems and the process that leads to the formation of terrestrial planets. Protoplanetary disks accrete their gas content and evolve into debris disks (produced by the collision of larger sized bodies) on a timescale of 10 million years. The signatures of debris disks appear as mid-infrared (mid-IR) excess emission. The fraction of stars displaying mid-IR excess and the magnitude of the excess appears to decrease with time. On top of this overall trend, a few individual stars show extremely large excesses even at several hundred million years. Determining the nature and frequency of the events producing those excesses promises to provide an important perspective on planetary system evolution.

The 30–150 Myr range is especially interesting since Canup (2004) and Touboul et al. (2007) showed that the Earth–Moon system was formed by a collision about 30–150 Myr after the solar system was formed. Gorlova et al. (2007) called attention to a ≈35 Myr old system with a large amount of debris that might have resulted from such a giant collision. Rhee et al. (2008), Gorlova et al. (2004), Rieke et al. (2005), and Su et al. (2006) also identify young debris systems with large 24 μm excesses.

NGC 2451A and B are two young open clusters projected on each other along the same line of sight that are within this interesting age range. Several attempts have been made to separate the two clusters and to determine the physical parameters of each one of them. Platais et al. (2001) analyzed photometric and spectroscopic data and used proper motions and radial velocities to select members of NGC 2451A. They fitted theoretical isochrones to the cluster color–magnitude diagram (CMD) to calculate its distance, reddening, and age. They derived $d = 188$ pc, $E(B-V) = 0.01$, and age = 60 Myr. Hünsch et al. (2003) carried out an X-ray study of the two clusters and identified 39 members of the A and 49 of the B cluster using combined X-ray and optical data. They derived distances of 206 pc and 370 pc, with corresponding ages of 50–80 Myr and 50 Myr for NGC 2451A and B, respectively. Hünsch et al. (2004) completed the X-ray study with high-resolution spectroscopy and refined the membership of the two clusters. The most recent distance and age estimate was performed by Kharchenko et al. (2005). They estimated distances of 188 pc and 430 pc and ages of 57.5 Myr and 75.9 Myr for NGC 2451A and B, respectively. However, their analysis was based on only a handful of member candidates (26 and 11 for NGC 2451A and B, respectively) in contrast with Hünsch et al. (2003). Therefore, we adopt the Hünsch et al. (2003) distances and ages and reddening ($E(B-V)$ of 0.01 and 0.05 for NGC 2451A and B, respectively) for our analysis.

In this paper, we report on a *Spitzer* IRAC and MIPS survey of the central region of the clusters to study the incidence of IR excesses in the 50–80 Myr age range. We supplement our *Spitzer* observations with a large-scale spectroscopic and optical photometric program to refine and extend our knowledge of the membership of these clusters.

2. OBSERVATIONS

2.1. Spitzer/*IRAC and MIPS Data*

Observations of NGC 2451 were obtained on 2004 March 2 with IRAC (Fazio et al. 2004). The IRAC survey covers about 0.6 deg^2 centered on HD 63032, a K2.5Ib star. The 12 s high-dynamic-range mode was used to obtain two frames in each position, one with 0.4 s exposure time and one with 10.4 s. The observation of each field was repeated twice with a small offset, providing 20.8 s integration time for each position. The frames were processed using the *Spitzer* Science Center IRAC Pipeline

[5] On leave from Department of Optics and Quantum Electronics, University of Szeged, H-6720 Szeged, Hungary.

v14.0, and mosaics were created from the basic calibrated data (BCD) frames using a custom IDL program (see Gutermuth et al. 2008 for details). Due to the 7 arcmin offset between channel 1/3 and channel 2/4, the total area covered in all four channels is about 0.45 deg^2.

Source finding and aperture photometry on these images were carried out using PhotVis version 1.10, which is an IDL–GUI-based photometry visualization tool (see Gutermuth et al. 2004 for further details on PhotVis). The radii of the source aperture, and of the inner and outer boundaries of the sky annulus, were 2.4, 2.4, and 7.2 arcsec, respectively. The calibration used large-aperture measurements of standard stars. The zero point magnitudes of the calibration were 19.6642, 18.9276, 16.8468, and 17.3909 corresponding to zero point fluxes of 280.9, 179.7, 115.0, and 64.13 Jy for channels 1, 2, 3, and 4, respectively. Aperture corrections of 0.21, 0.23, 0.35, and 0.5 mag were applied for channels 1, 2, 3, and 4 to account for the differences between the aperture sizes used for the standard stars and for the NGC 2451 photometry.

We accepted as good detections those with photometric uncertainties less than 0.2 mag, which allowed limiting magnitudes of 18.2, 17.5, 15.4, and 14.8 at 3.6 μm, 4.5 μm, 5.8 μm, and 8.0 μm, respectively. We detected almost 30,000 sources at 3.6 μm, more than 20,000 at 4.5 μm, and over 4000 and 3000 in the 5.8 μm and 8.0 μm images. There are more than 2500 sources that were detected in all four channels. Based on the Two Micron All Sky Survey magnitudes of the detected sources, the limiting mass of our survey is <0.1 $M_\odot$ for NGC 2451A and around 0.15 $M_\odot$ for NGC 2451B.

The MIPS (Rieke et al. 2004) 24 μm survey was obtained on 2004 April 11. It covers about 0.8 deg^2 centered on the same position as the IRAC survey. The observations were carried out in the scan map mode. The frames were processed using the MIPS Data Analysis Tool (Gordon et al. 2005). We used PhotVis to extract the sources in the 24 μm image and point-spread function (PSF) fitting in the IRAF/DAOPHOT package was used to obtain photometry. We used a 0.59 mag aperture correction and a 7.17 Jy zero point to convert our PSF photometry to the 24 μm magnitude scale. Similarly to the IRAC photometry we also discarded sources with errors larger than 0.2 mag, leaving 2625 sources in our MIPS sample. The limiting magnitude of our 24 μm survey is 11.8, which corresponds to masses of 0.55 $M_\odot$ (early M spectral type) and 0.9 $M_\odot$ (early K spectral type) for stars with pure photospheric emission at the distance of NGC 2451A and B, respectively.

Figure 1 shows the false color image of the center of NGC 2451.

2.2. Optical Photometry

The optical observations were made with the SITe 2048-6 CCD camera attached to the 1.5 m telescope at Cerro Tololo Inter-American Observatory (CTIO) on 2003 January 22, 23, and 24. The camera was mounted at the $f/13.5$ focal position, covering a 15 × 15 arcmin^2 field of view with a resolution of 0.43 arcsec/pixel for the entire 2048 × 2048 pixel^2 area. The observations were made through Johnson–Cousins *UBVRI* filters, from the Tek 1[6] filter set.

The whole cluster was covered by 4 × 3 = 12 CCD frames centered on and around the brightest inner area at R.A. = 07:45:20, decl. = −38:02:00. One off-cluster area (separated by ∼1.°5 from the cluster center) was also imaged to sample the galactic foreground/background object population in the same line of sight. Each field was imaged three times through the same filter. One frame was obtained with a short exposure time (10 s for *U* and 5 s for *BVRI*) and the other two frames were taken with a longer one (250 s for *U*, 70 s for *B*, and 50 s for *VRI*).

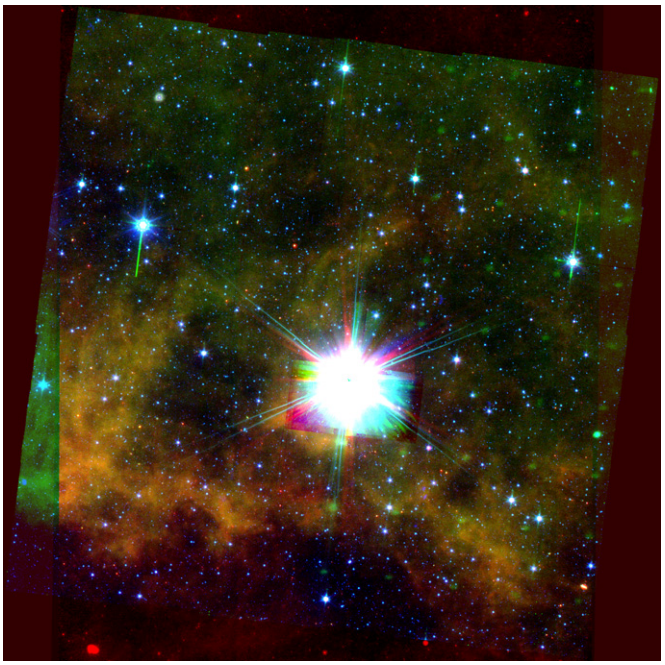

Figure 1. False color image of the center of NGC 2451. Blue: 4.5 μm; green: 8 μm; red: 24 μm.

(A color version of this figure is available in the online journal.)

The reductions of the raw frames were performed with standard routines using IRAF.[7] After trimming the edges of the frames and subtracting the bias level from each image, the frames were divided by a master flat-field image obtained by median combining the available flat-field frames for each filter. Both dome flats and sky flats were taken at the beginning of each night and combined together into the master flat frames. After flat-field division, the two long-exposure frames corresponding to the same filter were averaged to increase the signal-to-noise ratio (S/N).

The photometry of the cluster frames was computed via PSF-fitting using DAOPHOT implemented in IRAF. A second-order spatially variable PSF (`varorder=2`) was built for each frame to compensate for distortions of the PSFs due to either the optical imaging artifacts in the large field of view, or guiding errors that occurred randomly on a few frames. For the PSF-model, `function=auto` was selected, i.e., each built-in PSF function was computed and the best-fitting one was adopted automatically. In most cases, the `penny1` or the `penny2` function was the best-fitting one. The PSF stars were selected interactively from a sample of the ∼50 brightest, non-saturated stars on each frame, omitting the ones with suspicious profiles and/or detectable neighbors within $r = 15$ pixels. The `fitrad` parameter was set as 5 pixels corresponding roughly to the FWHM of the frames with the lowest quality. The detection threshold was fixed at the 4σ level on each frame.

[6] http://www.ctio.noao.edu/instruments/filters

[7] IRAF is distributed by the National Optical Astronomy Observatory, which is operated by the Association of Universities for Research in Astronomy, Inc., under cooperative agreement with the National Science Foundation.

Table 1
Transformation Coefficients Derived from Landolt Standards Observed on 2003 January 22

Coefficient	V	$(U-B)$	$(B-V)$	$(V-R)$	$(V-I)$
k	0.15	0.15	0.13	0.00	0.05
α	...	...	0.035	...	0.031
β	...	1.064	0.880	1.055	1.021
ζ	−2.457	−1.848	−0.133	−0.083	0.822

Table 2
Transformation Zero Points for the Three Nights

Date	ζ_V	ζ_{U-B}	ζ_{B-V}	ζ_{V-R}	ζ_{V-I}
2003 Jan 22	−2.457	−1.848	−0.133	−0.083	0.822
2003 Jan 23	−2.470	−1.770	−0.133	−0.083	0.800
2003 Jan 24	−2.486	−1.768	−0.134	−0.082	0.802

Inspecting the results of the PSF photometry revealed that there is a small, but significant, difference between the results of the PSF and aperture photometry of the same stellar field. This difference was about the same (within ∼0.03 mag) for the bright stars in one field, but its amount varied from field to field, ranging from a few hundredths up to ∼0.2 mag. The aperture photometry was computed with $r_{\rm ap} = 8$ pixels aperture radius (about 3.″4). The local sky level was estimated as the mode of the pixel distribution within an annulus having inner and outer radii of 10 and 20 pixels, respectively, centered on each object. Because $r_{\rm ap}$ was more than twice the stellar FWHM for most frames, much of this difference was probably due to the distorted stellar PSFs mentioned above, plus the problems in determining the local sky level during the PSF fitting. Therefore, we fixed the zero point of the photometry by selecting a bright, unsaturated, uncrowded reference star on each frame, and using its magnitude from aperture photometry as a reference level. Thus, the final instrumental magnitudes were determined as follows: first, differential magnitudes were computed between the PSF magnitudes of all stars and the reference object, then the magnitude of the reference object from aperture photometry was added to each differential magnitude. For the short-exposure frames, the same procedure was applied, but for the reference object the magnitudes from the long-exposure frames were selected, thus ensuring a common zero point for the photometry of the long- and short-exposure frames.

The transformation of the CTIO instrumental magnitudes into the standard Johnson–Cousins system was performed via observations of Landolt photometric standard sequences (Landolt 1992). The L98, L101, and RU152 standard fields were imaged through each filter, weather and time permitting, on each night at different airmasses (up to four different elevations in the case of the L98 field). Since photometric accuracy is essential for the conclusions of this paper, we give the details of our calibration and standard transformation below.

The following formulas were adopted for converting the instrumental magnitudes into standard ones:

$$V - (v - k_v X) = \alpha_{CI} \cdot CI + \zeta_V, \quad (1)$$

$$CI = \beta_{CI} \cdot (ci - k_{ci} X) + \zeta_{CI}, \quad (2)$$

where v and ci are the instrumental V-magnitude and color index ($u-b$, $b-v$, $v-r$, or $v-i$), V and CI are the standard magnitudes and colors, X is the airmass, ks are the extinction coefficients, α_{CI} and β_{CI} are the color-dependent transformation slopes (the color terms), and the ζs are the zero points.

Because the first night was nearly photometric, we decided to determine the color terms and the extinction coefficients from the magnitudes of standard stars observed that night. The instrumental magnitudes of these stars were computed from aperture photometry using the same aperture and annulus radii as mentioned above for the cluster frames. The transformation coefficients were then derived by fitting Equations (1) and (2) to the instrumental and standard magnitudes via χ^2 minimization. Table 1 lists the parameters for each filter combination (note that both $(B-V)$ and $(V-I)$ were applied as the color index in Equation (1)).

With the parameters listed in Table 1 determined, the color terms and extinction coefficients were kept fixed and only the zero points were fitted to the data for standard stars observed on the next two nights. Because we experienced slightly variable transparency during the second night, we have not attempted to adjust the extinction-correction coefficients to achieve the best fit. The variation of the zero points (collected together in Table 2) is under 0.01 mag except for $(U-B)$, illustrating the stability of the photometric conditions at the CTIO site during our observing run.

Inserting the coefficients from Tables 1 and 2 into Equations (1) and (2), the photometric data for the stars in the cluster fields have been transformed into the standard system. This resulted in a final sample of ∼29, 000 stars having calibrated photometry in at least the V and I filters with uncertainties less than 0.1 mag.

The quality and the stability of the whole photometry including the standard transformation have been verified by comparing our standard V and $B-V$ magnitudes with those from Platais et al. (2001) for the ∼1800 stars in common between the two samples. The agreement is very good. The mean difference between the two samples is 0.001 ± 0.06 mag in V and -0.007 ± 0.04 mag in $B-V$ (the errors are the rms of the residuals), thus, statistically insignificant. Therefore, our new CCD photometry in the field of NGC 2451 results in a sample containing ∼29, 000 stars with calibrated data. This nearly doubles the amount of photometric data available for this field.

2.3. Radial Velocity Survey

We acquired AAOmega data using the Anglo-Australian Telescope at Siding Spring, Australia on three nights, 2008 February 15, 16, and 17, in acceptable conditions (clear skies with 1.5–2.5 arcsec seeing). In the blue arm we used the 2500 V grating, providing $\lambda/\Delta\lambda = 8000$ spectra between 4800 Å and 5150 Å. In the red arm we used the 1700 D grating that has been optimized for recording the Ca II IR triplet region. The red spectra range from 8350 Å to 8790 Å, with $\lambda/\Delta\lambda = 10000$. This setup has the highest spectral resolution available with AAOmega, suitable to measure stellar radial velocities. In total, we acquired 11 field configurations centered on the open clusters. We selected the targets for our spectroscopic campaign based on their positions in the optical–near-IR CMD: we targeted each source that is brighter than the 80 Myr isochrone plus 0.2 mag placed at the distance of the more distant cluster in the V versus $V-K$ diagram. We show the spectroscopic candidates in Figure 2 together with all the stars with available V and K photometry in the field. Our spectroscopic coverage is not complete for two reasons: (1) we concentrated our efforts to the central part of the cluster where we had *Spitzer* data; (2) there were faint objects for which the low S/N of the spectra prevented measuring meaningful radial velocities.

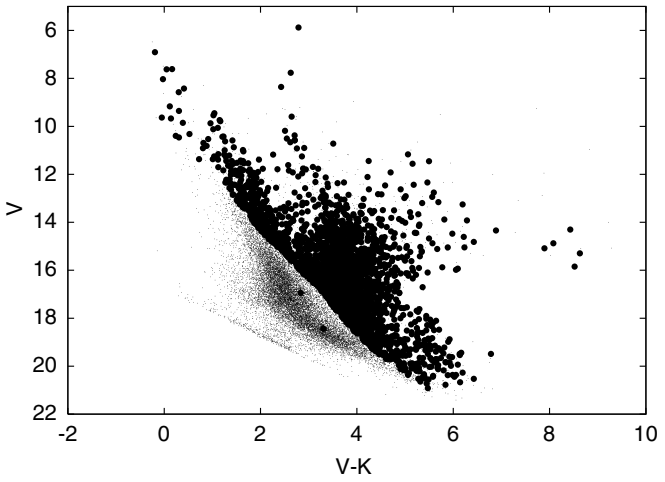

Figure 2. Spectroscopic sample on the V vs. $V-K$ diagram. Large dots: targets with spectra, small dots: all stars with available V and K magnitudes in the whole cluster area.

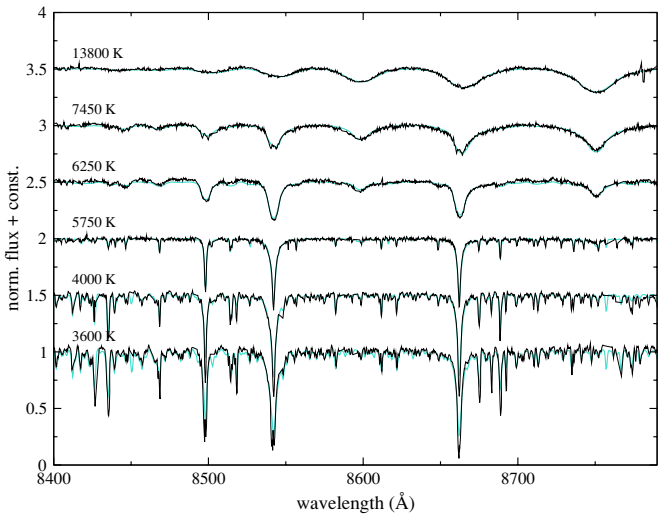

Figure 3. Observed stellar spectra (light blue/gray lines) and the best-fit synthetic data from the Munari et al. (2005) spectrum library (black lines).
(A color version of this figure is available in the online journal.)

The spectra were reduced using the standard Two-Degree Field data reduction pipeline. We performed continuum normalization for the stellar spectra using the IRAF task onedspec.continuum and then cleaned the strongest skyline residuals using linear interpolation of the surrounding continuum.

Atmospheric parameters and radial velocity were determined for each star in an iterative process, which combined finding best-fit synthetic spectrum from the Munari et al. (2005) spectrum library, with χ^2 fitting, and cross-correlating the best-fit model with the observed spectrum to calculate the radial velocity. This approach is very similar to that adopted by the Radial Velocity Experiment (RAVE) project (Steinmetz et al. 2006; Zwitter et al. 2008), and our analysis is based on the same synthetic library as RAVE. Earlier results for other star clusters with the same instrument and analysis can be found in Kiss et al. (2007, 2008). Because of the wide range of temperatures (and hence spectral features), we needed three subsequent iterations to converge to a stable set of temperatures, surface gravities, metallicities, and radial velocities. The latter are believed to be accurate within $\pm$1–2 km s^{-1} for the cooler stars and $\pm$5 km s^{-1} for the hotter stars in the sample (the boundary is roughly at 8000–9000 K). These values have been estimated from Gaussian fits of the cross-correlation profile using the IRAF task rv.fxcor and should only be considered as representative numbers. The atmospheric parameters ($T_{\rm eff}$, $[M/H]$, $\log g$), due to their degeneracy, are accurate to about $\pm$ 300 K and $\pm$ 0.5 dex, with strong correlations (see Zwitter et al. 2008 for a thorough discussion of the RAVE error analysis).

To illustrate the difficulties one faces when analyzing cool and hot stars together in the Ca II triplet region, we show sample spectral fits in Figure 3. Since the Ca II lines almost exactly coincide with hydrogen lines in the Paschen series, we found that it was absolutely crucial to have the best-match template for cross-correlation. A slight template mismatch can easily lead to radial velocity shifts of several km s^{-1} at this intermediate spectral resolution and hence one has to be very careful to optimize template selection (contrary to the commonly used practice in the optical range that the same template is used across a range of spectral subtypes or even types). It is also unavoidable that as soon as the temperature reaches about 9000 K, the broad spectral features will lead to a degraded velocity precision simply because of the broadened cross-correlation profile. NGC 2451A and B, as reasonably young open clusters, still host a significant number of hotter main-sequence stars, possibly resulting in degraded velocity precision for a fraction of stars.

Another difficulty was the very high incidence of Ca II emission (defined by the excess flux of the calcium lines relative to the best-fit model spectra), especially in late-type main-sequence stars in the clusters. Both clusters are young, hence the high rotation rates can lead to elevated chromospheric activity, for which the Ca II lines are good indicators (Andretta et al. 2005). When comparing the best-fit models to the observed spectra, we noticed distorted Ca II profiles for many stars, frequently in the form of central emission components within the lines. These can introduce random velocity errors of up to 10–20 km s^{-1} in the maximum of the cross-correlation profile. This was particularly apparent after modifying the velocity determination for 405 stars with Ca II line profile irregularities: after excluding the Ca II lines from cross-correlations, a large fraction of the refined velocities were very close to the cluster's mean velocities (Figure 4).

We also measured cross-correlation velocities from the lower resolution blue spectra. These data were less useful because many of the stars have a broad Hβ line and only a few additional weak features in the recorded wavelength range, leading to a broad cross-correlation profile and radial velocities accurate to only about $\pm$10 km s^{-1}.

3. ANALYSIS

3.1. Radial Velocities of the Clusters

The clusters are in the plane of the Milky Way so the background contamination overwhelms the cluster members. To estimate the radial velocities of the clusters, we need to make some assumptions to separate the probable cluster members from the field based on our present knowledge of the cluster. Based on the young age of the clusters, we assumed that our sample should contain a large number of K and M dwarfs that show chromospheric activity, i.e., signs of emission in the CaT lines. We identified 405 active red objects in our sample. Several of our target stars show sharp Hβ emission as additional evidence for activity. In the left panel of Figure 4, we show the

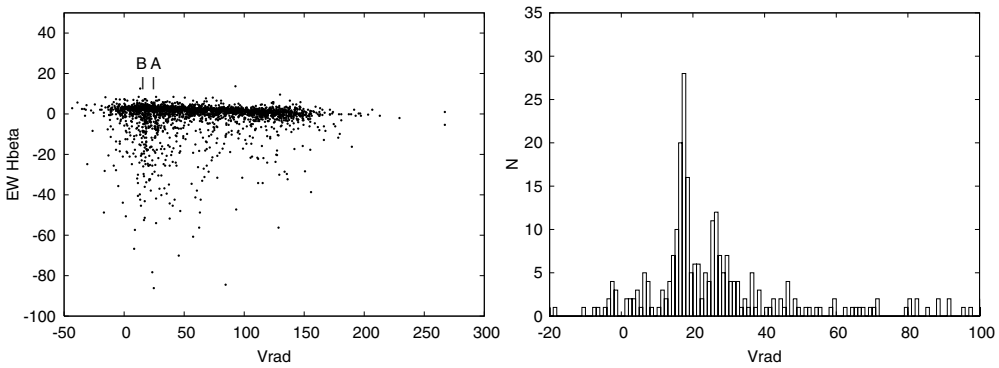

Figure 4. Left panel: EW of Hβ vs. radial velocity. A and B show the clusters' mean radial velocities from Hünsch et al. (2004). Left panel: all stars, right panel: radial velocity histogram of the two clusters using stars that show evidence of chromospheric activity.

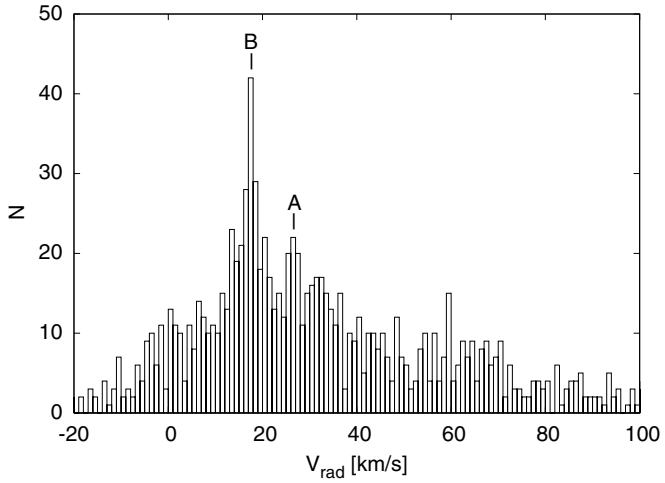

Figure 5. Radial velocity histogram of the two clusters using all stars with $\log g > 3.0$. A and B show the radial velocity values determined using the chromospherically active young stars for NGC 2451A and B, respectively.

equivalent width (EW) of Hβ versus radial velocity (negative EWs mean emission). We see two distinct groups of emission line objects in the figures around the approximate position of the radial velocity values of NGC 2451A and B (22.7 km s^{-1} and 14 km s^{-1}) that were estimated by Hünsch et al. (2004). We show the radial velocity histogram of these stars in the right panel of Figure 4. From this histogram, we calculate mean radial velocities 26.7 $\pm$ 2.4 km s^{-1} and 17.4 $\pm$ 2 km s^{-1} for NGC 2451A and B, respectively. Because chromospheric activity is not always present in young stars (e.g., early-type ones), we use this test only to estimate true cluster velocities.

Our average radial velocity values are about 3 km s^{-1} higher than those of Hünsch et al. (2004). Considering the formal standard deviation of the Hünsch et al. (2004) data (2.3 km s^{-1} for cluster A and 2.5 km s^{-1} for cluster B) and the small number of member stars in that sample (21 for cluster A and 10 for cluster B), the 3 km s^{-1} systematic difference is hardly significant. Given that our sample contains 3–10 times more members for each cluster, we adopt our mean values for the cluster velocities.

3.2. Cluster Membership and Color–Magnitude Diagrams

In Figure 5, we show the radial velocity histogram of our complete sample with $\log g > 3$ (giants filtered out). The two peaks at the positions of the radial velocities of the two clusters (designated with A and B) are readily distinguishable. However, a large number of contaminating stars might be present due to the strong galactic background, so the radial velocity is not enough to determine accurate membership status. Therefore, we used photometric diagrams also to clean our initial sample.

We performed the final determination of memberships as follows. We selected member candidates using the radial velocity and $\log g$ criteria. We accepted all objects as cluster members that had $\log g > 3$ (1079 out of 2570 objects satisfied this criterion) and not more than a 2σ deviation from the clusters' mean radial velocities (13.4 km s^{-1} $< V_{\rm rad} <$ 21.4 km s^{-1} for NGC 2451B and 21.9 km s^{-1} $< V_{\rm rad} <$ 31.5 km s^{-1} for NGC 2451A, 152 and 200 objects for NGC 2451A and B, respectively). Then we plotted the initial sample in CMDs and removed the objects with positions inconsistent with the 50 Myr isochrone of Siess et al. (2000) at the distance of the clusters. We show the final cleaned diagrams in Figure 6. Our final sample consists of 60 objects in NGC 2451A and 121 objects in NGC 2451B The photometry of the members is listed in Tables 3–6.

3.2.1. Members from Platais et al. (2001)

There are 18 members of NGC 2451A reported by Platais et al. (2001) in the area covered by all five bands of our *Spitzer* observations. Thirteen of them were included in our radial velocity survey. We rejected seven of these stars based on their radial velocity, four were included in our clean NGC 2451A membership list, while two have radial velocities just outside the 2σ limit. We included these two stars along with the other five not covered by the radial velocity survey in our final sample for NGC 2451A (they are marked with filled squares in the plots in the left column of Figure 6). We used the Platais et al. (2001) magnitudes for these objects because they were not detected by our *UBVRI* survey. As a result, they are not plotted in the V versus $V - I$ plot in Figure 6.

3.2.2. Members from Hünsch et al. (2003, 2004)

Hünsch et al. (2003) list 87 objects in the field of our *Spitzer* survey as candidate members of either NGC 2451A or B. Unfortunately, the coordinates given in Hünsch et al. (2003) are from X-ray data and have sufficiently large uncertainties that it is not easy to identify their sources in the IRAC and MIPS data sets. We could identify 58 sources out of 87 with a detection in at least one *Spitzer* band. Thirty four of them were included in our radial velocity survey which also included seven stars identified as non-members by Hünsch et al. (2003).

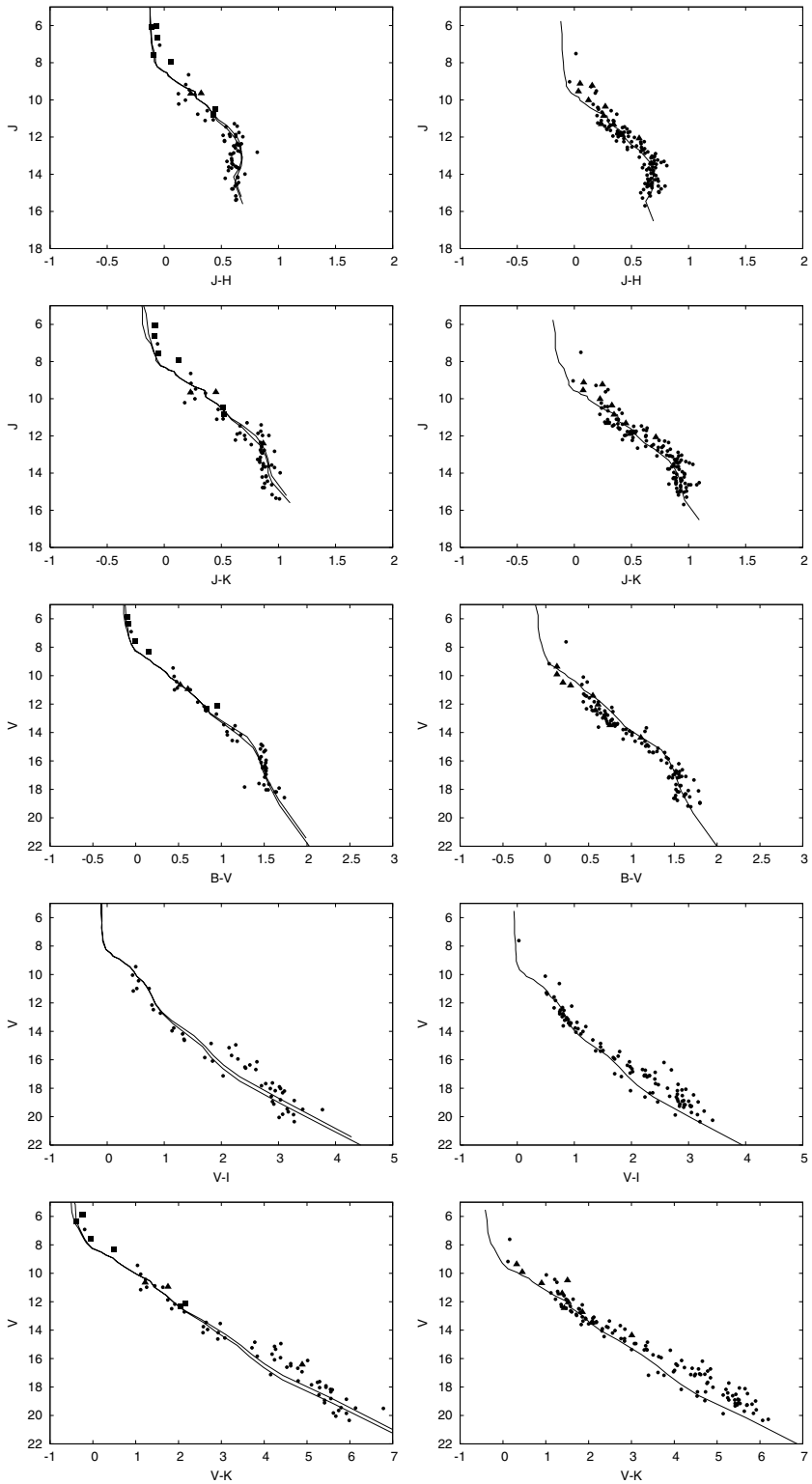

Figure 6. CMD of the members of the two clusters (left panel: NGC 2451A; right panel: NGC 2451B). Dots: stars in our spectroscopic survey; squares: members from Platais et al. (2001) not included in our spectroscopic sample; triangles: members from Hünsch et al. (2003) not included in our spectroscopic sample. The solid line shows the 50 Myr and 80 Myr isochrone of Siess et al. (2000) for NGC 2451A and the 50 Myr isochrone of Siess et al. (2000) for NGC 2451B, shifted with the distance and extinction of Hünsch et al. (2003).

In the case of NGC 2451A, 16 Hünsch et al. (2003) members are included in our radial velocity survey, which confirms the membership status of 10. In NGC 2451B, we have 13 Hünsch et al. (2003) members in our spectroscopic sample. Eight of them are confirmed as members by the radial velocity data, while two have radial velocities indicating that they are members of NGC 2451A. We can reject three Hünsch et al. (2003) members based on their radial velocity data. There is a third group of Hünsch et al. (2003) stars that contains objects that might be members of either of the clusters. Six of them are included in

our radial velocity survey. Based on the radial velocity data, we confirm membership of five objects (four in NGC 2451A and one in NGC 2451B). We included the Hünsch et al. (2003) members without radial velocities in our final sample if they were detected in at least one of the *Spitzer* bands (3 and 10 for NGC 2451A and B, respectively). They are marked with filled triangles in Figure 6. These additions make the total number of cluster members 69 and 131 for NGC 2451A and B, respectively. We detect 22 members at 24 μm, 47 at 8 and 4.5 μm, and 49 at 5.8 and 3.6 μm in NGC 2451A. In NGC 2451B, we detect 20 members at 24 μm, 92 at 8 μm, 96 at 5.8 μm, 94 at 4.5 μm, and 98 at 3.6 μm. Our detection rate in the IRAC bands is about 70% in both clusters, while at 24 μm it is 32% in NGC 2451A and 15% in NGC 2451B, respectively. These detection rates are very similar to that of Gorlova et al. (2007) for the ~35 Myr old cluster NGC 2457. In the following, we use only the sources that are detected in all four IRAC bands or detected at 24 μm.

4. IDENTIFYING EXCESS CANDIDATES

4.1. IRAC Excesses

The four IRAC bands covering the 3.6–8 μm regime of the spectrum trace dust from the near-sublimation temperature of 1000 to 400 K, corresponding to radii within 1 AU for solar-type stars. We can identify 8 μm excesses from the IRAC data, if we plot K-[8] versus $V-K$. Figure 7 shows the $V-K$ versus K-[8] color–color diagram of NGC 2451A (left panel) and B (right panel). The large baseline of the $V-K$ color makes this filter combination an ideal choice for photometric spectral type determination given the low reddening of the clusters. There is a monotonic relationship between increasing $V-K$ and stellar spectral type that results in a narrow locus, extending from early to late-type stars; the scatter in this locus increases for $V-K > 5$ due to measurement errors. Objects to the right of this locus are stars with excesses at 8 μm.

The robust determination of cluster membership allows us to establish a good color–color relation for 50–80 Myr clusters by fitting a second-degree polynomial to the locus of the $V-K$–K-[8] and $V-K$–K-[5.8] diagrams. We merged the data of the two clusters to increase the number of sources in the fit and required both colors of an A0 star to be 0. Equations (3) and (4) show the results of the fit which is also shown with a solid line on Figures 7 and 8. The rms of the datapoints around the fit is 0.05 in both colors:

$$(K_S-[8])_0 = 0.0115 \pm 0.0011(V-K_S)_0^2 - 5.89\times10^{-5} \pm 0.0053(V-K_S)_0, \quad (3)$$

$$(K_S-[5.8])_0 = 0.0125 \pm 0.0012(V-K_S)_0^2 - 0.0078 \pm 0.0060(V-K_S)_0. \quad (4)$$

No star with 8 μm excess (relative to K) was detected in NGC 2451A and only two candidate excess stars (1 and 2) and another two weak possible excess candidates (3 and 4) were detected in NGC 2451 B. We also plot the same diagrams but using the IRAC 5.8 μm channel on Figure 8. This diagram allows us to check whether our 8 μm detections are real or are just a result of some anomaly in the image (e.g., a cosmic ray hit). Both 8 μm excess candidates are confirmed by having excess at 5.8 μm also. However star 2 has a close companion that might compromise the 8 μm and 5.8 μm photometry (see Figure 9). Stars 3 and 4 are also situated slightly to the right of the main locus of sources in $V-K$ versus K-[5.8], however, 3 has a larger excess at 5.8 μm so its status as an excess candidate is questionable. None of the four 8 μm excess candidates were detected at 24 μm.

We fitted a Kurucz model to the short wavelength portion of the sources' spectral energy distributions (SEDs). Figure 10 shows the results of the fit. Based on their SEDs we can conclude that only one of the four candidates (1) is a true excess source. The SED of 2 shows that the photometry of this source is contaminated by the nearby bright star because the excess extends over all IRAC bands. The SED of 3 shows no excess at all and that of 4 has a marginal one. The significance of the excess for 4 calculated from the photometric errors and the rms of the fit is slightly lower than 3σ.

We noticed that there is a small hint of an 8 μm excess on the SED of the 24 μm excess star 12 (see the following section) and all but one of the A (or earlier) type stars have K-[8] colors less than zero although they are inside the 3σ limit of the trendline in Figure 7. To check the origin of this slight discrepancy we replaced K with [3.6] and used the $V-K$ versus [3.6]–[8.0] diagram to detect excesses (Figure 11). A linear relation between the $V-K$ and the [3.6]–[8.0] colors can be found for the photospheric sources

$$([3.6]-[8])_0 = 0.01842 \pm 0.001277(V-K_S)_0 \quad (5)$$

with rms scatter of 3%. We also show this relation along with the 3σ limits in Figure 11.

In this diagram, there is no systematic deviation from the main relation and it seems that 12 has a marginal excess at 8 μm relative to 3.6 μm. The significance of the excess is about 4σ. There are some excess candidates among the late M type stars of NGC 2451A but their significance is less than 3σ. In the case of NGC 2451B (Figure 11 right panel), the diagram clearly shows that the only viable 8 μm excess candidate is 1. Although 3 shows some [3.6]–[8.0] excess, the SED of the source does not support it.

To summarize, at 8 μm we have less than 2% excess fraction in NGC 2451A (one marginal excess) and a less than 1% excess fraction in NGC 2451B (one clean excess). This result is very similar to that of Gorlova et al. (2007) suggesting that IR excess shortward of 24 μm is very rare in clusters older than 20–30 Myr and indicates that the disk within 10 AU is cleared of dust for nearly all stellar systems older than 30 Myr.

4.2. MIPS Excesses

Figure 12 shows the dereddened $V-K$ versus K-[24] for NGC 2451A (left panel) and NGC 2451B (right panel). Because there are too few detections to determine a zero excess locus purely from these data, for this purpose we have used a database of more than 1500 stars derived from nearly all of the *Spitzer* debris disk programs. The sample has good coverage from $-0.4 < V-K < 3.5$, with still a number of members up to $V-K = 8$. A simple polynomial fit has been made to the photospheric color–color locus. The rms scatter around this fit (clipping the positive outliers that have excesses) is only 3%. The locus itself is therefore very well determined and we can take a typical uncertainty for the measurement of any given star to be 3% relative to this locus (plus any statistical errors). This locus with 3σ errors (9%) is plotted in Figure 12.

It is obvious that excess at 24 μm is far more common than at shorter wavelengths. We find 9 stars in the case of NGC 2451A and 10 stars in the case of NGC 2451B to the right of the

Table 3
UBVRIJHK Photometry of the Members of NGC 2451A

R.A. (J2000)	Decl. (J2000)	U (mag)	$\sigma(U)$ (mag)	B (mag)	$\sigma(B)$ (mag)	V (mag)	$\sigma(V)$ (mag)	R (mag)	$\sigma(R)$ (mag)	I (mag)	$\sigma(I)$ (mag)	J (mag)	$\sigma(J)$ (mag)	H (mag)	$\sigma(H)$ (mag)	K (mag)	$\sigma(K)$ (mag)
115.72653	−37.99071	...	...	...	...	19.841	0.043	18.399	0.017	16.579	0.014	14.793	0.031	14.201	0.038	13.917	0.059
115.73360	−38.35236	...	...	...	...	19.495	0.035	17.700	0.016	15.724	0.012	13.626	0.032	13.061	0.034	12.712	...
115.75735	−37.70676	...	...	...	...	19.095	0.036	17.701	0.017	16.180	0.009	14.628	0.032	14.010	0.033	13.685	0.060
115.77562	−37.69178	...	...	...	...	18.338	0.017	16.937	0.020	15.265	0.009	13.666	0.031	13.076	0.028	12.782	0.032
115.77648	−38.15585	17.636	0.013	16.611	0.006	15.152	0.008	14.158	0.010	13.017	0.008	11.758	0.023	11.104	0.020	10.912	0.021
115.80866	−38.21898	...	...	...	...	18.941	0.023	17.641	0.008	16.050	0.006	14.443	0.037	13.792	0.044	13.537	0.043
115.82023	−38.04878	...	...	...	...	19.826	0.046	18.482	0.013	16.752	0.009	15.153	0.043	14.527	0.059	14.209	0.069
115.84371	−37.73632	...	...	19.111	0.034	17.840	0.013	16.603	0.007	15.135	0.006	13.700	0.026	13.046	0.020	12.732	0.028
115.86862	−38.29049	...	...	...	...	19.471	0.041	18.046	0.013	16.319	0.008	14.551	0.026	13.915	0.024	13.673	0.053
115.91156	−38.23518	11.778	0.001	11.450	0.002	10.997	0.004	10.730	0.005	10.479	0.011	10.008	0.023	9.822	0.024	9.740	0.019
115.91624	−37.72572	...	...	17.166	0.008	15.702	0.003	14.643	0.003	13.527	0.003	12.361	0.025	11.683	0.020	11.519	0.023
115.91917	−38.11346	...	...	...	...	20.360	0.079	18.858	0.020	17.086	0.013	15.353	0.052	14.720	0.063	14.374	0.080
115.95297	−38.36620	...	...	16.833	0.019	15.337	0.004	...	...	...	...	11.987	0.021	11.298	0.026	11.069	0.017
115.96202	−38.11860	...	...	17.641	0.013	16.123	0.015	14.972	0.011	13.504	0.016	11.965	0.028	11.340	0.027	11.104	0.023
115.97014	−38.27538	17.413	0.011	16.422	0.006	14.939	0.006	13.902	0.004	12.684	0.005	11.405	0.021	10.764	0.022	10.555	0.019
115.97250	−37.95827	...	...	...	...	19.721	0.045	18.392	0.015	16.773	0.014	15.282	0.057	14.755	0.072	14.051	0.100
115.97843	−37.77519	18.779	0.041	17.984	0.008	16.505	0.006	15.407	0.005	14.095	0.003	12.765	0.023	12.101	0.020	11.889	0.021
115.98955	−38.46418	...	...	14.697	0.002	13.537	0.002	...	...	...	...	11.286	0.023	10.671	0.024	10.562	0.019
116.03289	−37.84594	17.328	0.010	16.305	0.003	14.840	0.004	13.925	0.006	13.015	0.005	11.877	0.021	11.252	0.022	11.056	0.021
116.04942	−37.73994 (6)	...	...	17.567	0.009	16.103	0.020	15.181	0.028	14.261	0.024	12.831	0.045	12.017	0.038	11.866	0.041
116.11263	−37.74447	...	...	...	...	20.063	0.054	18.823	0.023	17.052	0.008	15.400	0.051	14.774	0.059	14.391	0.088
116.13418	−37.68301	...	...	...	...	18.826	0.022	17.485	0.010	15.789	0.006	14.157	0.025	13.515	0.030	13.264	0.042
116.13475	−38.03229	11.692	0.003	11.622	0.005	10.985	0.004	10.634	0.008	10.246	0.008	9.714	0.021	9.446	0.022	9.351	0.019
116.14048	−38.15269	...	...	17.287	0.007	15.839	0.005	14.970	0.002	14.132	0.003	12.850	0.023	12.240	0.027	12.000	0.021
116.18760	−38.32344	...	...	...	...	19.484	0.058	17.932	0.010	16.059	0.005	14.209	0.025	13.675	0.026	13.351	0.038
116.20787	−38.16160	...	...	12.949	0.016	12.152	0.015	11.716	0.022	11.366	0.024	10.763	0.034	10.468	0.043	10.238	0.028
116.21219	−37.85936	13.672	0.002	13.310	0.002	12.486	0.001	12.072	0.005	11.673	0.004	11.109	0.025	10.751	0.030	10.650	0.024
116.21249	−37.74415	...	...	20.312	0.062	18.575	0.020	17.284	0.008	15.699	0.004	14.195	0.025	13.550	0.028	13.302	0.045
116.23017	−38.07956 (9)	...	...	...	...	11.160	0.006	10.931	0.006	10.702	0.006	10.218	0.019	10.092	0.020	10.039	0.019
116.25277	−37.53289	...	...	15.244	0.004	14.176	0.004	...	...	...	...	12.228	0.023	11.699	0.022	11.605	0.021
116.25701	−38.03892	...	...	10.508	0.003	10.059	0.005	9.817	0.003	9.614	0.004	9.182	0.018	8.992	0.020	8.947	0.023
116.27029	−38.07462	19.862	0.057	19.186	0.029	17.688	0.012	16.439	0.005	14.910	0.004	13.260	0.025	12.667	0.028	12.444	0.029
116.28444	−38.14332	...	...	15.410	0.003	14.181	0.007	13.469	0.013	12.859	0.003	11.965	0.019	11.388	0.022	11.261	0.021
116.29981	−37.79209	...	...	19.561	0.023	18.039	0.015	16.775	0.005	15.178	0.006	13.617	0.026	12.985	0.024	12.749	0.032
116.31223	−38.19624 (8)	10.882	0.007	10.905	0.003	10.424	0.007	10.155	0.006	9.874	0.008	9.467	0.058	9.249	0.077	9.192	0.062
116.33550	−37.89964	...	...	15.011	0.003	13.945	0.002	13.342	0.002	12.809	0.004	11.905	0.019	11.391	0.020	11.266	0.019
116.36404	−37.59628	...	...	6.857	0.002	6.909	0.001	...	...	...	...	7.045	0.013	7.086	0.021	7.101	0.005
116.38750	−37.51380	...	...	19.023	0.029	17.583	0.029	...	...	...	...	13.661	0.025	13.015	0.022	12.791	0.030
116.38871	−38.27644	...	...	19.821	0.026	18.180	0.013	16.889	0.005	15.241	0.004	13.574	0.021	12.951	0.024	12.632	0.030

Table 3
(Continued)

R.A. (J2000)	Decl. (J2000)	U (mag)	$\sigma(U)$ (mag)	B (mag)	$\sigma(B)$ (mag)	V (mag)	$\sigma(V)$ (mag)	R (mag)	$\sigma(R)$ (mag)	I (mag)	$\sigma(I)$ (mag)	J (mag)	$\sigma(J)$ (mag)	H (mag)	$\sigma(H)$ (mag)	K (mag)	$\sigma(K)$ (mag)
116.38876	−38.13771	...	...	14.901	0.002	13.763	0.006	13.124	0.005	12.598	0.002	11.846	0.023	11.274	0.020	11.184	0.019
116.39985	−37.77279	...	...	19.578	0.025	17.903	0.013	16.586	0.007	14.889	0.010	13.296	0.019	12.747	0.020	12.462	0.017
116.43397	−37.73853	19.867	0.055	18.637	0.015	17.131	0.013	16.144	0.009	15.103	0.013	13.998	0.026	13.291	0.022	12.981	0.029
116.44578	−37.93944	...	...	...	...	18.874	0.026	17.368	0.005	15.594	0.004	13.805	0.021	13.244	0.026	12.952	0.030
116.47578	−37.86585	...	...	19.828	0.027	18.197	0.012	16.821	0.005	15.093	0.005	13.481	0.026	12.880	0.028	12.612	0.029
116.48650	−37.80289	...	...	...	...	19.659	0.036	18.265	0.010	16.487	0.010	14.780	0.037	14.180	0.037	13.918	0.062
116.53485	−37.89772	...	...	17.475	0.006	15.952	0.006	14.920	0.005	13.666	0.006	12.433	0.019	11.774	0.020	11.572	0.019
116.54976	−38.10431	...	...	19.566	0.025	18.019	0.013	14.567	0.013	14.982	0.022	13.412	0.021	12.819	0.020	12.577	0.024
116.56485	−38.46915	...	...	18.459	0.046	16.935	0.012	...	...	...	...	12.909	0.019	12.332	0.026	12.054	0.023
116.60356	−38.01960	14.299	0.005	13.646	0.004	12.703	0.004	10.098	0.008	11.770	0.008	11.083	0.019	10.655	0.022	10.568	0.019
116.61087	−38.08359	16.206	0.008	15.690	0.010	14.564	0.014	11.761	0.013	13.218	0.016	12.189	0.023	11.663	0.026	11.480	0.021
116.62418	−37.87896	...	...	19.176	0.016	17.618	0.008	16.359	0.007	14.725	0.004	13.161	0.023	12.573	0.028	12.319	0.023
116.70172	−38.14828	...	...	9.890	0.001	9.453	0.000	9.191	0.012	8.953	0.001	8.642	0.017	8.431	0.029	8.411	0.039
116.74747	−38.37820 (7)	...	...	14.472	0.003	13.445	0.001	...	...	...	...	11.466	0.019	10.928	0.022	10.802	0.019
116.74952	−37.83876	19.006	0.018	18.121	0.007	16.602	0.005	15.521	0.004	14.177	0.004	12.934	0.023	12.344	0.022	12.074	0.021
116.76556	−37.95779	...	...	18.213	0.009	16.693	0.010	13.411	0.012	14.088	0.015	12.752	0.021	12.106	0.024	11.909	0.021
116.76661	−38.21130	17.462	0.052	17.865	0.013	16.360	0.007	15.242	0.003	13.862	0.003	12.592	0.025	11.968	0.022	11.740	0.021
116.77044	−38.22134	16.491	0.014	15.807	0.004	14.624	0.004	13.917	0.003	13.271	0.003	12.467	0.025	11.859	0.022	11.705	0.023
116.80532	−37.93312	...	...	16.750	0.016	15.238	0.006	...	...	...	...	12.384	0.021	11.736	0.020	11.527	0.023
116.87226	−37.88074	...	...	11.358	0.003	10.870	0.001	...	...	...	...	9.664	0.021	9.541	0.020	9.428	0.019
116.93404	−37.98419	...	...	12.585	0.002	11.860	0.002	...	...	...	...	10.580	0.021	10.204	0.020	10.109	0.021
Members from Platais et al. (2001)																	
115.92881	−38.20190	...	...	6.262	...	6.351	...	...	...	...	...	6.648	0.019	6.708	0.019	6.735	0.009
115.97642	−38.00076	13.632	0.002	13.150	0.003	12.309	0.002	...	...	11.373	0.010	10.817	0.021	10.385	0.020	10.296	0.019
116.14244	−37.94292	...	...	5.792	...	5.890	...	...	...	...	...	6.063	0.003	6.177	0.035	6.146	0.017
116.18701	−38.05376 (12)	...	...	7.570	...	7.580	...	...	...	...	...	7.583	0.019	7.676	0.049	7.637	0.025
116.24871	−38.09417	...	...	8.458	...	8.304	...	...	...	...	...	7.929	0.005	7.869	0.027	7.805	0.019
116.54395	−37.93366	...	...	5.776	...	5.870	...	...	...	...	...	6.030	0.009	6.100	0.037	6.107	0.011
116.75196	−37.84372	...	...	13.013	0.045	11.898	0.061	11.366	0.066	10.795	0.073	10.469	0.021	10.018	0.024	9.951	0.024
Members from Hünsch et al. (2003)																	
116.02866	−37.98943	...	...	17.94	...	16.43	...	...	...	...	...	12.409	0.025	11.772	0.022	11.542	0.023
116.10025	−38.59977 (11)	...	...	11.562	0.002	10.953	0.001	...	...	...	...	9.648	0.023	9.325	0.026	9.196	0.017
116.53718	−37.39910 (10)	...	...	11.18	...	10.66	...	...	...	...	...	9.669	0.019	9.437	0.020	9.439	0.021

Note. Numbers next to the coordinates designate 24 μm excess sources from Table 7.
(This table is also available in a machine-readable form in the online journal.)

Table 4
UBVRIJHK Photometry of the Members of NGC 2451B

R.A. (J2000)	Decl. (J2000)	U (mag)	$\sigma(U)$ (mag)	B (mag)	$\sigma(B)$ (mag)	V (mag)	$\sigma(V)$ (mag)	R (mag)	$\sigma(R)$ (mag)	I (mag)	$\sigma(I)$ (mag)	J (mag)	$\sigma(J)$ (mag)	H (mag)	$\sigma(H)$ (mag)	K (mag)	$\sigma(K)$ (mag)
115.72778	−37.95026	16.698	0.014	15.763	0.005	14.607	0.010	13.908	0.020	13.281	0.025	12.465	0.018	11.919	0.020	11.773	0.019
115.75046	−37.79300	19.520	0.072	18.393	0.020	16.887	0.007	15.726	0.006	14.473	0.004	13.047	0.026	12.345	0.026	12.106	0.024
115.75243	−37.95836	13.070	0.009	12.958	0.004	12.332	0.008	11.940	0.013	11.542	0.019	11.140	0.025	10.794	0.020	10.757	0.023
115.77086	−37.81706	12.230	0.004	12.070	0.002	11.563	0.002	11.199	0.002	10.918	0.004	10.425	0.023	10.217	0.020	10.134	0.019
115.77200	−37.98902	18.918	0.042	17.743	0.009	16.189	0.007	15.040	0.009	13.623	0.012	12.358	0.025	11.774	0.020	11.533	0.023
115.79673	−38.09564	...	...	15.036	0.003	14.024	0.004	13.427	0.008	12.869	0.007	12.031	0.021	11.503	0.020	11.406	0.019
115.79724	−38.15298	17.356	0.012	16.408	0.005	15.099	0.007	14.359	0.008	13.644	0.008	12.551	0.023	11.965	0.020	11.772	0.017
115.80643	−37.79030	...	...	20.087	0.084	18.473	0.020	17.077	0.007	15.387	0.007	13.659	0.026	13.062	0.028	12.764	0.032
115.82157	−38.28752	...	...	20.142	0.066	18.634	0.016	17.547	0.015	16.400	0.013	15.002	0.059	14.347	0.075	14.100	0.073
115.82535	−37.76639	...	...	19.925	0.069	18.409	0.021	17.095	0.007	15.607	0.005	14.057	0.031	13.343	0.030	13.162	0.030
115.83157	−38.09364	14.138	0.004	13.923	0.004	13.163	0.005	12.720	0.010	12.272	0.026	11.676	0.028	11.297	0.032	11.069	0.024
115.85167	−37.93698	...	...	14.240	0.006	13.407	0.006	12.918	0.003	12.464	0.006	11.843	0.021	11.429	0.020	11.313	0.019
115.86620	−37.92305	...	...	19.519	0.034	18.000	0.013	16.808	0.008	15.371	0.009	13.967	0.028	13.296	0.020	13.097	0.037
115.86779	−37.94924	...	...	15.193	0.005	14.188	0.006	13.609	0.004	13.075	0.009	12.257	0.023	11.757	0.020	11.628	0.021
115.86904	−38.05129	...	...	19.969	0.053	18.345	0.016	17.246	0.008	16.020	0.009	14.782	0.031	14.020	0.026	13.803	0.059
115.86959	−37.94765	...	...	...	...	19.879	0.056	18.684	0.022	17.108	0.012	15.694	0.078	15.074	0.082	14.735	0.133
115.87277	−37.75060	...	...	7.850	0.014	7.614	0.029	7.436	0.049	7.589	0.016	7.510	0.015	7.495	0.029	7.454	0.015
115.87687	−38.35557	...	...	13.305	0.012	12.520	0.012	12.134	0.011	11.705	0.007	11.109	0.029	10.813	0.040	10.740	0.036
115.90090	−37.87689	...	...	20.297	0.093	18.762	0.021	17.461	0.009	15.961	0.006	14.444	0.040	13.765	0.020	13.513	0.043
115.91875	−38.14002	...	...	13.582	0.002	12.891	0.004	12.508	0.020	12.081	0.007	11.563	0.023	11.277	0.024	11.180	0.023
115.93221	−37.69007	...	...	14.352	0.004	13.544	0.001	13.051	0.005	12.620	0.003	11.985	0.023	11.600	0.020	11.544	0.021
115.94174	−37.91011	...	...	20.711	0.160	18.913	0.035	17.501	0.012	15.911	0.008	14.389	0.028	13.740	0.026	13.501	0.037
115.95562	−37.89574 (14)	...	...	11.049	0.026	10.627	0.020	10.198	0.038	9.890	0.052	9.637	0.028	9.453	0.026	9.364	0.021
115.95767	−38.21386	17.695	0.011	16.570	0.006	15.366	0.006	14.657	0.006	13.991	0.006	13.079	0.025	12.512	0.026	12.358	0.026
115.96495	−38.22524	19.851	0.072	18.476	0.019	16.991	0.009	16.088	0.008	15.288	0.007	14.262	0.035	13.533	0.026	13.372	0.041
115.98142	−38.18655	14.021	0.006	13.747	0.006	13.045	0.008	12.582	0.011	12.176	0.006	11.590	0.021	11.303	0.022	11.194	0.017
115.98473	−37.77708	19.327	0.063	18.293	0.012	16.733	0.006	15.663	0.007	14.491	0.005	13.084	0.031	12.404	0.028	12.169	0.028
115.99301	−37.62355	...	...	12.443	0.001	11.826	0.001	...	...	...	...	10.579	0.023	10.257	0.020	10.186	0.021
116.01189	−38.12175	...	...	18.681	0.018	17.096	0.011	16.040	0.006	14.866	0.007	13.479	0.031	12.868	0.030	12.606	0.033
116.01443	−38.12092	...	...	20.111	0.049	18.615	0.024	17.378	0.008	15.829	0.007	14.212	0.031	13.537	0.027	13.251	0.036
116.03135	−37.74863	...	...	...	...	18.849	0.023	17.565	0.009	15.938	0.005	14.295	0.050	13.631	0.053	13.364	0.053
116.04131	−37.91467	...	...	14.189	0.003	13.396	0.006	12.930	0.007	12.471	0.005	11.758	0.021	11.289	0.020	11.217	0.023
116.06585	−37.76541	18.603	0.030	17.563	0.007	16.150	0.005	15.204	0.005	14.188	0.004	12.885	0.028	12.175	0.024	11.975	0.021
116.08724	−37.88116	...	...	18.700	0.019	17.140	0.009	16.049	0.008	14.826	0.005	13.418	0.026	12.737	0.027	12.524	0.026
116.09396	−37.88209	...	...	13.915	0.002	13.148	0.003	12.725	0.005	12.293	0.004	11.741	0.023	11.305	0.022	11.222	0.021
116.09680	−37.92455	11.746	0.003	11.841	0.002	11.381	0.004	11.150	0.004	10.856	0.006	10.502	0.021	10.289	0.022	10.263	0.021
116.12193	−37.77896	13.539	0.002	13.459	0.002	12.780	0.002	12.387	0.004	11.989	0.005	11.383	0.021	11.070	0.022	10.962	0.021
116.13069	−37.72335	...	...	18.664	0.014	17.185	0.006	16.228	0.005	15.360	0.006	14.286	0.031	13.579	0.035	13.422	0.042
116.13331	−37.74069	...	...	19.974	0.048	18.337	0.019	17.243	0.009	15.967	0.006	14.625	0.051	13.890	0.073	13.608	0.068
116.15142	−37.81565	19.207	0.040	18.199	0.011	16.677	0.006	15.653	0.005	14.485	0.005	13.120	0.040	12.450	0.035	12.259	0.043
116.15163	−37.90051	...	...	14.245	0.001	13.444	0.003	12.994	0.004	12.520	0.004	11.763	0.021	11.352	0.026	11.258	0.021
116.15218	−38.40723	...	...	14.863	0.015	13.887	0.005	...	...	...	...	12.080	0.021	11.645	0.022	11.568	0.019
116.15345	−37.91661	...	...	18.553	0.026	17.112	0.008	16.043	0.018	14.884	0.012	13.600	0.029	12.915	0.029	12.729	0.028
116.15422	−37.82180	18.934	0.035	17.845	0.007	16.376	0.006	15.431	0.005	14.450	0.004	13.241	0.023	12.513	0.024	12.341	0.026

Table 4
(Continued)

R.A. (J2000)	Decl. (J2000)	U (mag)	$\sigma(U)$ (mag)	B (mag)	$\sigma(B)$ (mag)	V (mag)	$\sigma(V)$ (mag)	R (mag)	$\sigma(R)$ (mag)	I (mag)	$\sigma(I)$ (mag)	J (mag)	$\sigma(J)$ (mag)	H (mag)	$\sigma(H)$ (mag)	K (mag)	$\sigma(K)$ (mag)
116.16007	−37.86702	...	...	...	...	20.366	0.078	19.004	0.022	17.164	0.007	15.290	0.069	14.694	0.063	14.309	0.094
116.17784	−38.18400	...	...	14.696	0.002	13.795	0.004	13.260	0.004	12.730	0.004	11.969	0.026	11.496	0.030	11.342	0.026
116.17909	−37.68557	...	...	...	...	20.267	0.065	18.728	0.019	16.843	0.007	14.997	0.039	14.415	0.053	14.073	0.070
116.18128	−38.30692	...	...	18.738	0.020	17.199	0.009	16.134	0.004	14.930	0.003	13.637	0.023	12.928	0.020	12.725	0.023
116.18606	−37.80272	...	...	19.693	0.032	18.154	0.014	16.907	0.007	15.350	0.005	13.776	0.026	13.143	0.027	12.945	0.026
116.20740	−38.13024	...	...	11.720	0.003	11.275	0.004	11.020	0.005	10.762	0.012	10.233	0.023	10.068	0.020	9.996	0.019
116.20831	−38.33110	...	...	19.185	0.026	17.662	0.020	16.496	0.019	15.237	0.012	13.803	0.028	13.110	0.028	12.886	0.032
116.21406	−38.13371	...	...	14.704	0.003	13.768	0.006	13.231	0.005	12.751	0.007	11.856	0.019	11.459	0.020	11.347	0.024
116.21574	−38.16710	19.726	0.055	18.489	0.022	16.936	0.030	15.945	0.022	14.961	0.028	13.775	0.029	13.106	0.030	12.956	0.036
116.21670	−38.28414	...	...	16.030	0.005	14.849	0.005	14.137	0.005	13.389	0.005	12.269	0.028	11.687	0.033	11.477	0.026
116.21722	−38.06004	17.118	0.012	16.667	0.006	15.410	0.011	14.652	0.008	13.954	0.012	12.774	0.023	12.193	0.022	12.047	0.021
116.21815	−37.99622	18.349	0.019	17.290	0.007	15.858	0.006	14.960	0.004	14.178	0.003	13.028	0.021	12.346	0.022	12.220	0.019
116.21956	−37.96960	...	...	20.921	0.117	19.227	0.036	17.869	0.011	16.202	0.007	14.504	0.052	13.888	0.059	13.410	0.059
116.23083	−37.78915	...	...	...	...	19.335	0.037	18.055	0.009	16.423	0.008	14.814	0.038	14.209	0.053	13.917	0.058
116.24108	−38.02993	...	...	...	...	19.110	0.027	17.808	0.007	16.264	0.006	14.616	0.018	13.966	0.032	13.616	0.046
116.26111	−38.03118	13.142	0.003	13.184	0.002	12.495	0.004	12.098	0.002	11.744	0.003	11.108	0.018	10.769	0.020	10.723	0.023
116.26560	−38.10297	...	...	13.505	0.003	12.782	0.004	12.392	0.002	12.035	0.002	11.356	0.019	11.037	0.022	10.976	0.019
116.26915	−37.94337	17.773	0.012	16.810	0.006	15.422	0.005	14.534	0.004	13.629	0.003	12.255	...	11.641	...	11.512	0.023
116.27896	−38.20475	18.211	0.015	17.283	0.005	15.938	0.006	15.080	0.004	14.235	0.003	13.085	0.021	12.392	0.026	12.241	0.019
116.28159	−37.66232	...	...	14.090	0.053	13.371	0.018	...	...	...	...	11.957	0.019	11.619	0.026	11.505	0.019
116.28564	−38.28589	...	...	20.188	0.040	18.509	0.017	17.233	0.006	15.617	0.004	14.031	0.026	13.333	0.028	13.068	0.037
116.29492	−38.32831	...	...	19.728	0.029	18.174	0.014	17.200	0.006	16.190	0.005	14.938	0.043	14.199	0.050	14.013	0.063
116.30032	−37.75469	14.114	0.003	13.927	0.004	13.211	0.007	12.784	0.004	12.379	0.009	11.764	0.021	11.378	0.022	11.273	0.019
116.30482	−37.83787	12.816	0.010	12.822	0.005	12.347	0.009	12.032	0.010	11.700	0.017	11.248	0.021	11.045	0.024	10.980	0.021
116.30806	−37.78869	...	...	19.309	0.018	17.744	0.010	16.617	0.004	15.276	0.006	13.931	0.021	13.242	0.028	12.984	0.032
116.32416	−37.81474	13.744	0.002	13.632	0.002	12.967	0.004	12.577	0.003	12.180	0.004	11.639	0.023	11.323	0.024	11.245	0.021
116.32484	−37.82308	14.232	0.002	14.233	0.002	13.619	0.005	13.232	0.004	12.816	0.004	12.212	0.021	11.843	0.028	11.793	0.026
116.33729	−37.83136	12.353	0.006	12.406	0.004	11.840	0.004	11.511	0.006	11.169	0.006	10.664	0.019	10.421	0.020	10.369	0.017
116.34253	−38.16618	...	...	19.725	0.023	18.063	0.016	16.754	0.005	15.107	0.006	13.446	0.023	12.784	0.020	12.541	0.024
116.34356	−38.06953	...	...	...	...	19.271	0.034	17.979	0.008	16.426	0.006	14.731	0.032	14.053	0.035	13.801	0.047
116.36942	−38.19338	...	...	...	...	19.282	0.028	17.863	0.027	16.246	0.014	14.559	0.036	13.909	0.043	13.589	0.049
116.37029	−38.09812	...	...	...	...	18.904	0.023	17.558	0.006	16.015	0.004	14.265	0.073	13.621	0.037	13.394	0.038
116.38677	−37.85640	20.094	0.053	19.315	0.021	17.737	0.011	16.477	0.005	14.919	0.008	13.355	0.019	12.682	0.020	12.469	0.023
116.39377	−37.86470	14.490	0.004	14.222	0.003	13.383	0.005	12.921	0.003	12.463	0.005	11.771	0.023	11.374	0.024	11.306	0.024
116.39548	−37.83491	...	...	...	...	19.610	0.040	18.156	0.012	16.334	0.010	14.581	0.034	13.920	0.033	13.691	0.053
116.39838	−37.91670	...	...	...	...	17.080	0.009	15.976	0.005	14.829	0.004	13.412	0.025	12.716	0.026	12.491	0.021
116.40154	−37.77890	17.754	0.010	16.632	0.009	15.334	0.009	14.551	0.006	13.831	0.005	12.797	0.023	12.152	0.028	11.983	0.026
116.40282	−37.94396	...	...	...	...	18.582	0.022	17.336	0.006	15.917	0.006	14.385	0.026	13.648	0.024	13.443	0.049
116.40669	−37.50750	...	...	13.859	0.002	13.084	0.002	...	...	...	...	11.479	0.021	11.058	0.026	10.960	0.024
116.44107	−37.89720 (17)	...	...	14.167	0.002	13.360	0.004	12.872	0.002	12.314	0.004	11.465	0.018	11.027	0.020	10.877	0.017
116.45256	−37.54667	...	...	9.207	0.005	9.168	0.002	...	...	...	...	9.041	0.017	9.082	0.022	9.053	0.021
116.46779	−38.52593	...	...	16.118	0.009	14.950	0.003	...	...	...	...	12.619	0.018	12.004	0.022	11.854	0.024
116.48573	−37.95175	...	...	...	...	19.160	0.037	17.852	0.007	16.218	0.006	14.517	0.035	13.879	0.030	13.625	0.050
116.49277	−37.99629	13.171	0.022	12.993	0.010	12.222	0.013	9.650	0.022	11.268	0.029	10.782	0.023	10.409	0.020	10.365	0.023
116.50293	−37.67097	...	...	12.724	0.001	12.195	0.001	...	...	...	...	11.125	0.025	10.891	0.024	10.836	0.023
116.50903	−37.86043	15.997	0.006	14.849	0.004	13.677	0.005	13.051	0.003	12.476	0.003	11.578	0.019	11.117	0.020	10.943	0.023
116.50935	−38.07950	...	...	20.780	0.038	18.979	0.014	15.439	0.012	15.813	0.022	14.048	0.026	13.412	0.035	13.081	0.035

Table 4
(Continued)

R.A. (J2000)	Decl. (J2000)	U (mag)	$\sigma(U)$ (mag)	B (mag)	$\sigma(B)$ (mag)	V (mag)	$\sigma(V)$ (mag)	R (mag)	$\sigma(R)$ (mag)	I (mag)	$\sigma(I)$ (mag)	J (mag)	$\sigma(J)$ (mag)	H (mag)	$\sigma(H)$ (mag)	K (mag)	$\sigma(K)$ (mag)
116.51448	−38.01421	...	...	20.828	0.047	19.171	0.016	15.728	0.008	16.250	0.017	14.674	0.038	14.036	0.041	13.745	0.056
116.54938	−38.21002	14.470	0.002	14.198	0.006	13.407	0.004	12.938	0.006	12.508	0.006	11.839	0.031	11.466	0.040	11.329	0.034
116.56459	−37.74740	19.043	0.020	17.928	0.015	16.468	0.009	15.515	0.009	14.495	0.011	13.272	0.021	12.571	0.020	12.394	0.021
116.57994	−37.56290	...	...	15.891	0.029	14.770	0.009	...	...	...	...	12.561	0.023	12.097	0.020	11.935	0.019
116.58564	−37.96366	...	...	...	...	19.706	0.020	16.238	0.009	16.659	0.010	15.028	0.044	14.374	0.050	14.068	0.073
116.60560	−38.23373	...	...	...	...	18.975	0.050	17.921	0.025	16.514	0.011	15.175	0.038	14.511	0.065	14.264	0.088
116.61145	−38.10934	...	...	19.886	0.023	18.104	0.011	14.648	0.010	15.220	0.012	13.468	0.018	12.752	0.024	12.459	0.019
116.66325	−38.32594	...	...	...	...	18.903	0.054	17.660	0.014	16.083	0.009	14.518	0.029	13.846	0.040	13.628	0.059
116.66850	−38.04359	19.475	0.021	18.212	0.006	16.620	0.010	13.479	0.013	14.611	0.017	13.315	0.065	12.531	0.064	12.379	0.053
116.67281	−37.84615	19.480	0.027	18.350	0.009	16.828	0.006	15.833	0.004	14.808	0.003	13.668	0.021	13.016	0.026	12.816	0.028
116.67488	−37.98390 (13)	20.007	0.033	18.738	0.010	17.101	0.009	13.842	0.014	14.785	0.016	13.369	0.023	12.609	0.022	12.393	0.024
116.68185	−38.28975	15.533	0.006	14.996	0.004	14.056	0.005	13.520	0.003	13.026	0.004	12.251	0.019	11.816	0.022	11.744	0.024
116.68972	−37.82607	13.385	0.002	13.275	0.002	12.637	0.003	12.264	0.004	11.893	0.003	11.405	0.018	11.138	0.022	11.058	0.019
116.69822	−38.00890	...	...	...	...	19.840	0.025	16.320	0.018	16.685	0.023	14.974	0.036	14.231	0.046	13.991	0.068
116.72084	−37.71950	19.244	0.021	18.233	0.009	16.714	0.004	15.530	0.003	14.014	0.003	12.712	0.019	12.109	0.024	11.870	0.017
116.72728	−37.59192	...	...	16.163	0.015	14.964	0.005	...	...	...	...	12.630	0.021	12.037	0.020	11.893	0.021
116.73331	−38.35595	...	...	10.554	0.009	10.117	0.001	9.896	0.012	9.626	0.002	9.289	0.019	9.142	0.020	9.099	0.021
116.74249	−37.63916 (18)	...	...	12.272	0.001	11.835	0.001	...	...	...	...	10.836	0.018	10.635	0.020	10.611	0.017
116.75339	−37.96264	...	...	...	...	19.255	0.017	15.751	0.012	16.204	0.013	14.627	0.045	13.833	0.041	13.556	0.060
116.76585	−37.96487	...	...	19.078	0.013	17.349	0.010	14.052	0.011	14.943	0.014	13.536	0.032	12.727	0.032	12.500	0.035
116.77636	−37.73380	18.212	0.012	17.143	0.009	15.735	0.007	14.843	0.008	13.970	0.009	13.062	0.025	12.362	0.020	12.231	0.024
116.79779	−37.79682	...	...	12.978	0.002	12.437	0.002	...	...	...	...	11.274	0.023	11.046	0.022	10.968	0.023
116.81857	−38.30363	...	...	11.909	0.001	11.437	0.001	...	...	...	...	10.414	0.019	10.210	0.022	10.147	0.019
116.84155	−38.30055	...	...	16.654	0.017	15.407	0.006	...	...	...	...	12.872	0.023	12.254	0.024	12.108	0.026
116.84765	−37.71917	...	...	15.081	0.012	13.926	0.004	...	...	...	...	11.711	0.024	11.226	0.036	11.080	0.026
116.86294	−38.13213	...	...	18.606	0.080	17.172	0.022	...	...	...	...	14.602	0.039	13.932	0.036	13.774	0.050
116.92513	−38.18621	...	...	15.655	0.003	14.615	0.003	...	...	...	...	12.534	0.037	12.030	0.049	11.857	0.035
116.94233	−38.15534	...	...	13.326	0.001	12.727	0.001	...	...	...	...	11.461	0.021	11.158	0.020	11.128	0.021
116.94269	−37.51560	...	...	15.373	0.044	14.468	0.014	...	...	...	...	12.659	0.021	12.193	0.022	12.105	0.024
116.94462	−37.88126	...	...	10.917	0.002	10.434	0.001	...	...	...	...	9.522	0.019	9.330	0.025	9.228	0.019
Members from Hünsch et al. (2003)																	
115.95710	−37.96688	...	...	10.025	0.001	9.855	0.001	9.736	0.009	9.682	0.013	9.547	0.023	9.511	0.020	9.470	0.019
116.03583	−37.98349	9.346	0.001	9.466	0.001	9.359	0.001	9.386	0.004	9.291	0.005	9.132	0.031	9.082	0.020	9.050	0.023
116.07976	−38.00541	...	...	15.48	...	14.37	...	...	...	...	...	12.076	0.023	11.508	0.022	11.362	0.017
116.15953	−38.22106	...	...	10.70	...	10.50	...	...	...	...	...	9.239	0.023	9.083	0.024	8.993	0.017
116.20300	−38.09869	...	...	14.24	...	13.49	...	...	...	...	...	11.899	0.019	11.478	0.024	11.410	0.023
116.21267	−37.66869 (15)	...	...	10.99	...	10.70	...	...	...	...	...	10.022	0.019	9.898	0.022	9.797	0.023
116.36051	−38.19643 (19)	12.030	0.009	11.997	0.002	11.438	0.005	11.137	0.004	10.816	0.004	10.366	0.026	10.095	0.022	10.037	0.021
116.38235	−37.50727	...	...	13.43	...	12.73	...	...	...	...	...	11.327	0.025	10.983	0.033	10.876	0.028
116.39170	−37.79194	13.020	0.003	12.996	0.005	12.425	0.007	12.112	0.004	11.784	0.005	11.310	0.019	11.073	0.022	11.020	0.021
116.50776	−38.00752 (16)	12.613	0.001	12.723	0.002	12.041	0.003	11.696	0.001	11.384	0.002	10.863	0.021	10.606	0.022	10.515	0.019

Note. Numbers next to the coordinates designate 24 μm excess sources from Table 7.
(This table is also available in a machine-readable form in the online journal.)

Table 5
Spitzer 3.6 μm–24 μm Photometry of Members of NGC 2451A

R.A. (J2000)	Decl. (J2000)	[3.6] (mag)	σ([3.6]) (mag)	[4.5] (mag)	σ([4.5]) (mag)	[5.8] (mag)	σ([5.8]) (mag)	[8.0] (mag)	σ([8.0]) (mag)	[24] (mag)	σ([24]) (mag)
115.72653	−37.99071	...	...	...	...	...	...	...	...	...	...
115.73360	−38.35236	...	...	...	...	...	...	...	...	...	...
115.75735	−37.70676	...	...	...	...	...	...	...	...	...	...
115.77562	−37.69178	...	...	...	...	...	...	...	...	...	...
115.77648	−38.15585	...	...	...	...	...	...	...	...	...	...
115.80866	−38.21898	...	...	...	...	...	...	...	...	...	...
115.82023	−38.04878	...	...	...	...	...	...	...	...	...	...
115.84371	−37.73632	...	...	...	...	...	...	...	...	...	...
115.86862	−38.29049	...	...	...	...	...	...	...	...	...	...
115.91156	−38.23518	...	...	...	...	...	...	...	...	...	...
115.91624	−37.72572	11.362	0.004	11.394	0.005	11.296	0.014	11.301	0.020	...	...
115.91917	−38.11346	14.216	0.014	14.111	0.021	14.038	0.096	13.916	0.147	...	...
115.95297	−38.36620	10.988	0.004	...	...	10.938	0.011	...	...	...	...
115.96202	−38.11860	10.906	0.004	10.868	0.004	10.822	0.010	10.830	0.014	10.489	0.055
115.97014	−38.27538	10.380	0.003	10.379	0.003	10.363	0.008	10.309	0.008	...	...
115.97250	−37.95827	14.134	0.014	14.086	0.023	14.559	0.128	...	...	...	...
115.97843	−37.77519	11.722	0.005	11.684	0.006	11.675	0.016	11.597	0.019	...	...
115.98955	−38.46418	...	...	...	...	...	...	...	...	10.401	0.054
116.03289	−37.84594	10.944	0.003	10.939	0.004	10.819	0.010	10.849	0.013	...	...
116.04942	−37.73994 (6)	11.616	0.005	11.581	0.005	11.497	0.016	11.527	0.021	10.767	0.073
116.11263	−37.74447	14.175	0.015	14.081	0.022	13.986	0.102	13.812	0.124	...	...
116.13418	−37.68301	13.068	0.008	12.948	0.011	12.971	0.044	12.976	0.062	...	...
116.13475	−38.03229	9.382	0.002	9.403	0.003	9.374	0.005	9.365	0.005	9.245	0.034
116.14048	−38.15269	11.922	0.005	11.950	0.007	11.881	0.022	11.828	0.035	...	...
116.18760	−38.32344	13.070	0.008	...	...	12.990	0.046	...	...	...	...
116.20787	−38.16160	10.252	0.003	10.205	0.003	10.222	0.007	10.180	0.008	10.161	0.051
116.21219	−37.85936	10.638	0.003	10.695	0.004	10.671	0.009	10.647	0.014	10.708	0.067
116.21249	−37.74415	13.037	0.009	12.987	0.010	12.916	0.047	12.941	0.061	...	...
116.23017	−38.07956 (9)	10.033	0.003	9.995	0.003	10.038	0.007	9.963	0.007	9.465	0.036
116.25277	−37.53289	...	...	...	...	...	...	...	...	...	...
116.25701	−38.03892	8.970	0.002	8.981	0.003	8.914	0.005	9.039	0.005	9.012	0.033
116.27029	−38.07462	12.226	0.007	12.145	0.008	12.139	0.022	12.110	0.041	...	...
116.28444	−38.14332	11.223	0.004	11.278	0.005	11.199	0.012	11.210	0.018	11.209	0.141
116.29981	−37.79209	12.534	0.006	12.477	0.008	12.413	0.027	12.439	0.039	...	...
116.31223	−38.19624 (8)	9.193	0.003	9.162	0.004	9.136	0.005	9.137	0.004	8.645	0.046
116.33550	−37.89964	11.210	0.004	11.219	0.005	11.138	0.023	11.135	0.014	...	...
116.36404	−37.59628	...	...	7.220	0.002	...	...	7.189	0.002	7.230	0.031
116.38750	−37.51380	...	...	...	...	...	...	...	...	...	...
116.38871	−38.27644	12.409	0.006	...	...	12.271	0.027	...	...	...	...

Table 5
(Continued)

R.A. (J2000)	Decl. (J2000)	[3.6] (mag)	σ([3.6]) (mag)	[4.5] (mag)	σ([4.5]) (mag)	[5.8] (mag)	σ([5.8]) (mag)	[8.0] (mag)	σ([8.0]) (mag)	[24] (mag)	σ([24]) (mag)
116.38876	−38.13771	11.174	0.004	11.205	0.005	11.210	0.013	11.179	0.018	...	...
116.39985	−37.77279	12.182	0.005	12.145	0.007	12.004	0.021	12.057	0.033	...	...
116.43397	−37.73853	12.945	0.008	12.946	0.011	12.915	0.037	12.959	0.064	...	...
116.44578	−37.93944	12.669	0.007	12.620	0.008	12.502	0.036	12.574	0.048	...	...
116.47578	−37.86585	12.499	0.006	12.224	0.009	12.217	0.027	12.144	0.041	...	...
116.48650	−37.80289	13.630	0.011	13.542	0.013	13.509	0.059	13.538	0.089	...	...
116.53485	−37.89772	11.425	0.004	11.422	0.005	11.362	0.014	11.341	0.018	...	...
116.54976	−38.10431	12.338	0.006	12.214	0.007	12.181	0.025	12.254	0.036	...	...
116.56485	−38.46915	...	...	...	...	...	...	...	...	...	...
116.60356	−38.01960	10.537	0.003	10.612	0.004	10.502	0.009	10.481	0.011	10.510	0.073
116.61087	−38.08359	11.453	0.004	11.471	0.005	11.436	0.015	11.413	0.015	...	...
116.62418	−37.87896	12.131	0.006	12.064	0.007	12.075	0.021	12.005	0.036	...	...
116.70172	−38.14828	8.436	0.002	8.416	0.002	8.415	0.003	8.409	0.003	8.260	0.031
116.74747	−38.37820 (7)	...	...	...	...	...	...	...	...	10.154	0.060
116.74952	−37.83876	11.890	0.005	11.850	0.006	11.768	0.018	11.779	0.034	...	...
116.76556	−37.95779	11.713	0.004	11.662	0.005	11.580	0.016	11.589	0.021	...	...
116.76661	−38.21130	11.541	0.004	11.534	0.005	11.492	0.015	11.472	0.031	...	...
116.77044	−38.22134	11.669	0.004	11.734	0.006	11.629	0.016	11.649	0.025	...	...
116.80532	−37.93312	11.465	0.004	11.479	0.005	11.417	0.014	11.378	0.021	...	...
116.87226	−37.88074	...	...	...	...	...	...	...	...	...	...
116.93404	−37.98419	...	...	...	...	...	...	...	...	...	...
Members from Platais et al. (2001)											
115.92881	−38.20190	6.835	0.002	6.856	0.002	6.892	0.002	6.811	0.001	...	...
115.97642	−38.00076	10.367	0.003	10.306	0.004	10.274	0.008	10.261	0.010	10.113	0.052
116.14244	−37.94292	6.267	0.002	6.271	0.002	6.329	0.001	6.275	0.001	6.305	0.031
116.18701	−38.05376 (12)	7.694	0.002	7.684	0.002	7.633	0.002	7.582	0.002	6.033	0.031
116.24871	−38.09417	7.880	0.002	7.916	0.002	7.902	0.003	7.856	0.002	7.844	0.032
116.54395	−37.93366	6.181	0.002	6.149	0.002	6.174	0.001	6.158	0.001	6.206	0.031
116.75196	−37.84372	9.880	0.002	9.901	0.003	9.851	0.006	9.815	0.006	9.814	0.045
Members from Hünsch et al. (2003)											
116.02866	−37.98943	11.336	0.004	11.271	0.005	11.192	0.013	11.207	0.018	...	...
116.10025	−38.59977 (11)	...	...	...	...	...	...	...	...	8.961	0.038
116.53718	−37.39910 (10)	...	...	...	...	...	...	...	...	9.171	0.038

Note. Numbers next to the coordinates designate 24 μm excess sources from Table 7.
(This table is also available in a machine-readable form in the online journal.)

Table 6
Spitzer 3.6 μm–24 μm Photometry of Members of NGC 2451B

R.A. (J2000)	Decl. (J2000)	[3.6] (mag)	σ([3.6]) (mag)	[4.5] (mag)	σ([4.5]) (mag)	[5.8] (mag)	σ([5.8]) (mag)	[8.0] (mag)	σ([8.0]) (mag)	[24] (mag)	σ([24]) (mag)
115.72778	−37.95026	...	...	...	...	...	...	...	...	...	...
115.75046	−37.79300	...	...	...	...	...	...	...	...	...	...
115.75243	−37.95836	...	...	...	...	...	...	...	...	...	...
115.77086	−37.81706	...	...	...	...	...	...	...	...	...	...
115.77200	−37.98902	...	...	...	...	...	...	...	...	...	...
115.79673	−38.09564	...	...	...	...	...	...	...	...	...	...
115.79724	−38.15298	...	...	...	...	...	...	...	...	...	...
115.80643	−37.79030	...	...	...	...	...	...	...	...	...	...
115.82157	−38.28752	...	...	...	...	...	...	...	...	...	...
115.82535	−37.76639	...	...	...	...	...	...	...	...	...	...
115.83157	−38.09364	...	...	...	...	...	...	...	...	...	...
115.85167	−37.93698	...	...	...	...	...	...	...	...	...	...
115.86620	−37.92305	...	...	...	...	...	...	...	...	...	...
115.86779	−37.94924	...	...	...	...	...	...	...	...	...	...
115.86904	−38.05129	...	...	...	...	...	...	...	...	...	...
115.86959	−37.94765	...	...	...	...	...	...	...	...	...	...
115.87277	−37.75060	7.541	0.002	7.547	0.002	7.515	0.002	7.563	0.002	...	...
115.87687	−38.35557	...	...	...	...	...	...	...	...	...	...
115.90090	−37.87689	13.309	0.009	13.271	0.012	13.328	0.047	13.257	0.089	...	...
115.91875	−38.14002	11.166	0.003	11.186	0.004	11.152	0.013	11.213	0.016	...	...
115.93221	−37.69007	...	...	11.534	0.005	...	...	11.488	0.020	...	...
115.94174	−37.91011	13.250	0.010	13.170	0.012	13.205	0.047	13.166	0.054	...	...
115.95562	−37.89574 (14)	9.343	0.002	9.373	0.003	9.310	0.005	9.308	0.004	8.549	0.034
115.95767	−38.21386	12.271	0.005	12.329	0.007	12.285	0.025	12.284	0.039	...	...
115.96495	−38.22524	13.292	0.009	13.379	0.013	13.277	0.048	13.476	0.086	...	...
115.98142	−38.18655	11.225	0.004	11.204	0.005	11.237	0.013	11.165	0.016	...	...
115.98473	−37.77708	12.048	0.006	12.052	0.007	11.980	0.021	11.922	0.033	...	...
115.99301	−37.62355	...	...	10.193	0.003	...	...	10.141	0.009	10.300	0.048
116.01189	−38.12175	12.425	0.007	12.425	0.009	12.372	0.025	12.417	0.043	...	...
116.01443	−38.12092	13.103	0.008	13.044	0.014	12.937	0.032	13.123	0.073	...	...
116.03135	−37.74863	13.200	0.009	13.131	0.013	12.974	0.040	13.169	0.088	...	...
116.04131	−37.91467	11.110	0.004	11.071	0.004	11.042	0.011	11.066	0.015	...	...
116.06585	−37.76541	11.889	0.005	11.840	0.006	11.798	0.016	11.778	0.032	...	...
116.08724	−37.88116	12.359	0.006	12.348	0.007	12.303	0.025	12.307	0.039	...	...
116.09396	−37.88209	11.148	0.004	11.183	0.005	11.116	0.012	11.132	0.018	...	...
116.09680	−37.92455	10.259	0.003	10.334	0.004	10.236	0.008	10.210	0.008	10.229	0.062
116.12193	−37.77896	10.950	0.003	10.973	0.004	10.929	0.011	10.903	0.014	...	...
116.13069	−37.72335	13.300	0.009	13.337	0.012	13.171	0.044	13.421	0.081	...	...
116.13331	−37.74069	13.008	0.025	12.923	0.034	12.936	0.078	12.797	0.065	...	...
116.15142	−37.81565	12.066	0.005	12.044	0.007	12.059	0.024	11.992	0.036	...	...
116.15163	−37.90051	11.229	0.004	11.224	0.005	11.138	0.014	11.184	0.014	...	...
116.15218	−38.40723	11.502	0.004	...	...	11.435	0.016	...	...	...	...
116.15345	−37.91661	12.568	0.007	12.576	0.009	12.383	0.024	12.582	0.047	...	...

Table 6
(Continued)

R.A. (J2000)	Decl. (J2000)	[3.6] (mag)	σ([3.6]) (mag)	[4.5] (mag)	σ([4.5]) (mag)	[5.8] (mag)	σ([5.8]) (mag)	[8.0] (mag)	σ([8.0]) (mag)	[24] (mag)	σ([24]) (mag)
116.15422	−37.82180	12.238	0.006	12.215	0.007	12.116	0.023	12.206	0.046	...	...
116.16007	−37.86702	14.124	0.015	14.029	0.019	14.097	0.088	...	...	...	...
116.17784	−38.18400	11.244	0.004	11.278	0.005	11.233	0.013	11.279	0.016	...	...
116.17909	−37.68557	13.816	0.012	13.784	0.015	13.806	0.076	13.748	0.119	...	...
116.18128	−38.30692	12.564	0.006	...	...	12.451	0.028	...	...	...	...
116.18606	−37.80272	12.694	0.007	12.653	0.008	12.619	0.031	12.696	0.046	...	...
116.20740	−38.13024	9.980	0.002	9.911	0.003	9.925	0.007	9.908	0.007	9.932	0.042
116.20831	−38.33110	12.683	0.007	...	...	12.591	0.034	...	...	...	...
116.21406	−38.13371	11.306	0.004	11.252	0.005	11.251	0.014	11.249	0.016	...	...
116.21574	−38.16710	12.728	0.007	12.709	0.009	12.663	0.032	12.553	0.048	...	...
116.21670	−38.28414	11.407	0.004	11.406	0.005	11.324	0.013	11.374	0.017	...	...
116.21722	−38.06004	11.936	0.005	11.940	0.006	11.905	0.022	11.927	0.049	...	...
116.21815	−37.99622	12.130	0.008	12.150	0.008	12.090	0.034	12.054	0.050	...	...
116.21956	−37.96960	13.577	0.027	13.396	0.017	...	...	13.642	0.130	...	...
116.23083	−37.78915	13.732	0.011	13.670	0.017	13.632	0.084	13.783	0.126	...	...
116.24108	−38.02993	13.476	0.016	13.386	0.023	13.265	0.051	...	...	...	...
116.26111	−38.03118	10.668	0.004	10.707	0.004	10.687	0.014	10.628	0.038	...	...
116.26560	−38.10297	10.927	0.003	10.948	0.004	10.889	0.011	10.936	0.013	...	...
116.26915	−37.94337	11.415	0.006	11.381	0.032	11.323	0.031	11.344	0.040	...	...
116.27896	−38.20475	12.141	0.005	12.104	0.007	12.039	0.021	12.041	0.036	...	...
116.28159	−37.66232	11.530	0.004	11.485	0.005	11.555	0.017	11.457	0.026	...	...
116.28564	−38.28589	12.848	0.007	...	...	12.711	0.032	...	...	...	...
116.29492	−38.32831	13.914	0.014	...	...	13.883	0.087	...	...	...	...
116.30032	−37.75469	11.290	0.004	11.319	0.005	11.398	0.014	11.271	0.018	...	...
116.30482	−37.83787	10.996	0.003	10.998	0.004	11.039	0.012	10.957	0.016	...	...
116.30806	−37.78869	12.918	0.008	12.807	0.009	12.701	0.032	12.839	0.045	...	...
116.32416	−37.81474	11.223	0.004	11.257	0.005	11.217	0.013	11.241	0.019	...	...
116.32484	−37.82308	11.778	0.005	11.802	0.006	11.777	0.017	11.725	0.024	...	...
116.33729	−37.83136	10.373	0.003	10.353	0.003	10.383	0.008	10.319	0.008	10.624	0.066
116.34253	−38.16618	12.272	0.006	12.273	0.007	12.169	0.023	12.144	0.035	...	...
116.34356	−38.06953	13.550	0.010	13.512	0.014	13.515	0.081	13.531	0.100	...	...
116.36942	−38.19338	13.407	0.009	13.342	0.012	13.361	0.057	13.269	0.077	...	...
116.37029	−38.09812	12.924	0.008	12.995	0.011	13.111	0.064	12.889	0.049	...	...
116.38677	−37.85640	12.246	0.005	12.193	0.007	12.095	0.019	12.194	0.048	...	...
116.39377	−37.86470	11.217	0.004	11.271	0.005	11.270	0.014	11.227	0.014	...	...
116.39548	−37.83491	13.450	0.012	13.252	0.012	13.283	0.056	13.254	0.086	...	...
116.39838	−37.91670	12.237	0.007	12.423	0.012	...	...	12.508	0.093	...	...
116.40154	−37.77890	11.915	0.005	11.944	0.006	11.837	0.018	11.981	0.029	...	...
116.40282	−37.94396	13.175	0.008	13.212	0.013	13.662	0.077	13.289	0.082	...	...
116.40669	−37.50750	...	...	...	...	...	...	...	...	...	...
116.44107	−37.89720 (17)	10.869	0.003	10.849	0.004	10.871	0.011	10.733	0.012	10.368	0.049
116.45256	−37.54667	...	...	9.088	0.003	...	...	9.057	0.004	8.977	0.038
116.46779	−38.52593	...	...	...	...	...	...	...	...	...	...
116.48573	−37.95175	13.559	0.010	13.329	0.013	13.270	0.054	13.560	0.088	...	...
116.49277	−37.99629	10.329	0.003	10.338	0.003	10.336	0.008	10.311	0.009	10.326	0.062

Table 6
(Continued)

R.A. (J2000)	Decl. (J2000)	[3.6] (mag)	σ([3.6]) (mag)	[4.5] (mag)	σ([4.5]) (mag)	[5.8] (mag)	σ([5.8]) (mag)	[8.0] (mag)	σ([8.0]) (mag)	[24] (mag)	σ([24]) (mag)
116.50293	−37.67097	10.801	0.003	10.819	0.004	10.805	0.010	10.725	0.013	...	...
116.50903	−37.86043	10.913	0.003	10.987	0.004	10.915	0.011	10.879	0.014	...	...
116.50935	−38.07950	12.816	0.007	12.745	0.009	12.697	0.038	12.680	0.050	...	...
116.51448	−38.01421	13.498	0.009	13.419	0.013	13.381	0.045	13.579	0.080	...	...
116.54938	−38.21002	11.339	0.005	11.312	0.005	11.275	0.014	11.218	0.016	11.221	0.127
116.56459	−37.74740	12.325	0.006	12.312	0.007	12.339	0.028	12.239	0.037	...	...
116.57994	−37.56290	...	...	11.977	0.006	...	...	11.911	0.031	...	...
116.58564	−37.96366	13.892	0.013	13.785	0.019	13.788	0.088	13.711	0.122	...	...
116.60560	−38.23373	14.052	0.013	13.853	0.016	13.681	0.076	13.519	0.083	...	...
116.61145	−38.10934	12.265	0.005	12.198	0.007	12.130	0.025	12.139	0.037	...	...
116.66325	−38.32594	13.385	0.009	...	...	13.300	0.058	...	...	...	...
116.66850	−38.04359	12.217	0.006	12.233	0.008	12.193	0.027	12.147	0.050	...	...
116.67281	−37.84615	12.832	0.007	12.574	0.008	12.434	0.029	12.514	0.043	...	...
116.67488	−37.98390 (13)	12.227	0.005	12.230	0.007	12.081	0.021	12.105	0.041	10.955	0.072
116.68185	−38.28975	11.682	0.004	...	...	11.726	0.018	...	...	...	...
116.68972	−37.82607	11.071	0.004	11.073	0.004	11.063	0.011	11.020	0.014	...	...
116.69822	−38.00890	13.726	0.011	13.540	0.014	13.406	0.057	13.888	0.158	...	...
116.72084	−37.71950	11.653	0.004	11.633	0.006	11.616	0.019	11.574	0.022	...	...
116.72728	−37.59192	...	...	11.864	0.006	...	...	11.802	0.025	...	...
116.73331	−38.35595	9.071	0.003	...	...	...	...	...	...	9.068	0.039
116.74249	−37.63916 (18)	10.586	0.003	10.587	0.004	10.589	0.009	10.578	0.010	10.302	0.059
116.75339	−37.96264	13.379	0.010	13.279	0.012	13.266	0.053	13.330	0.081	...	...
116.76585	−37.96487	12.370	0.006	12.367	0.008	12.292	0.027	12.268	0.043	...	...
116.77636	−37.73380	12.111	0.006	12.096	0.008	12.045	0.023	12.120	0.040	...	...
116.79779	−37.79682	...	...	...	...	...	...	...	...	...	...
116.81857	−38.30363	10.169	0.002	...	...	10.152	0.007	...	...	...	...
116.84155	−38.30055	12.075	0.005	...	...	12.043	0.022	...	...	...	...
116.84765	−37.71917	...	...	...	...	...	...	...	...	...	...
116.86294	−38.13213	...	...	...	...	...	...	...	...	...	...
116.92513	−38.18621	...	...	...	...	...	...	...	...	...	...
116.94233	−38.15534	...	...	...	...	...	...	...	...	...	...
116.94269	−37.51560	...	...	...	...	...	...	...	...	...	...
116.94462	−37.88126	...	...	...	...	...	...	...	...	...	...
Members from Hünsch et al. (2003)											
115.95710	−37.96688	9.491	0.002	9.460	0.003	9.460	0.005	9.456	0.006	9.345	0.036
116.03583	−37.98349	9.044	0.003	9.059	0.003	9.044	0.004	9.011	0.004	9.073	0.032
116.07976	−38.00541	11.294	0.004	11.269	0.005	11.215	0.013	11.226	0.018	...	...
116.15953	−38.22106	9.010	0.002	8.985	0.003	8.932	0.004	8.922	0.004	8.839	0.033
116.20300	−38.09869	11.365	0.004	11.459	0.005	11.417	0.015	11.325	0.018	...	...
116.21267	−37.66869 (15)	...	...	9.797	0.003	9.883	0.007	9.755	0.005	9.285	0.034
116.36051	−38.19643 (19)	10.036	0.003	10.056	0.003	10.017	0.007	10.029	0.007	9.704	0.038
116.38235	−37.50727	...	...	...	...	...	...	...	...	10.648	0.069
116.39170	−37.79194	11.008	0.004	11.017	0.004	10.964	0.011	10.953	0.014	10.912	0.069
116.50776	−38.00752 (16)	10.562	0.004	10.540	0.004	10.495	0.009	10.474	0.010	9.983	0.043

Note. Numbers next to the coordinates designate 24 μm excess sources from Table 7.
(This table is also available in a machine-readable form in the online journal.)

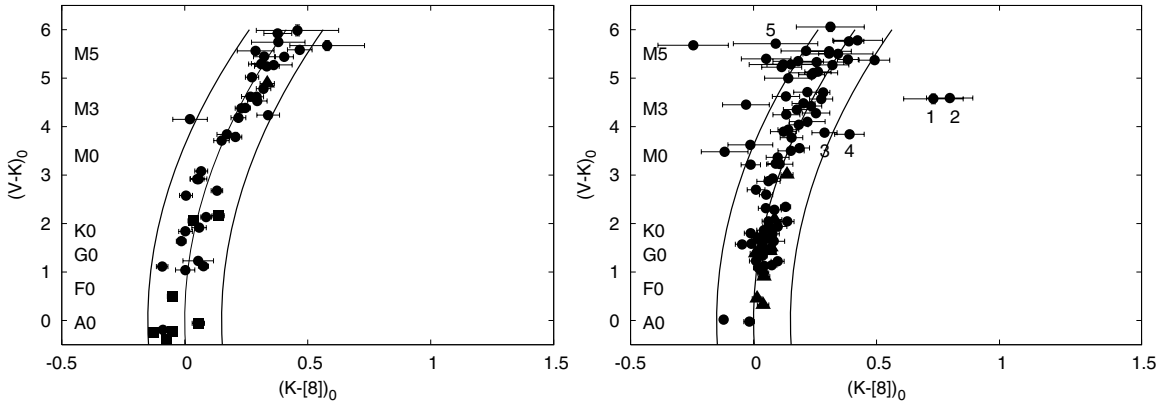

Figure 7. $V - K$ vs. K-[8] diagrams of NGC 2451A (left panel) and B (right panel). The meaning of the symbols is the same as in Figure 6. Horizontal error bars show the 1σ photometric errors. The solid lines represent the color–color relation for normal stars and its 3σ limits.

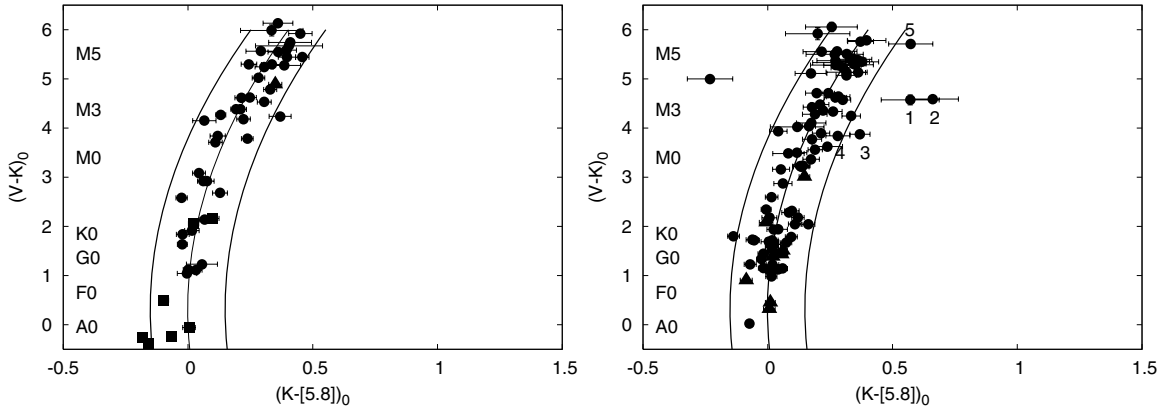

Figure 8. Same as Figure 7 but for $V - K$ vs. K-[5.8].

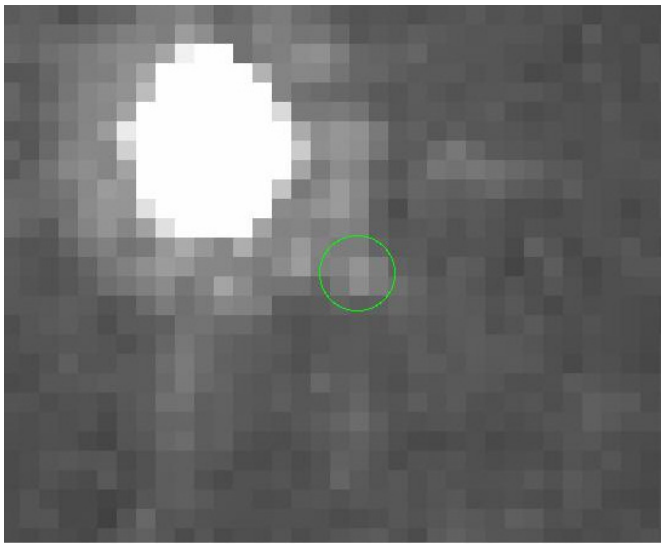

Figure 9. Location of star 2. The green circle shows the aperture size that was used for the photometry.

(A color version of this figure is available in the online journal.)

photospheric locus. However, only 7 of them in both diagrams (the numbered sources in Figure 12) are more than 3σ distance from the locus (the distance of the negative outlier left of the locus). The measured $(K\text{-}[24])_0$ color along with the predicted photospheric K-[24] color of these objects and the significance of the excesses are presented in Table 7. For the prediction of the photospheric colors we used the photospheric locus shown in Figure 12. The significance was calculated using the photometric errors and the rms around this locus. To check the validity of our excess candidates (as in the previous section), we fit Kurucz model atmospheres to the short-wavelength part of their SEDs. The fits are shown in Figures 13 and 14. In all cases the 24 μm flux is above the photosphere by more than 3σ, confirming the excess. The fraction of stars with excess at 24 μm is about $33\% \pm 10\%$ (7/22) for NGC 2451A and $36\% \pm 10\%$ (7/20) for NGC 2451B. We calculated the disk fractions and errors using Bayesian statistics as described in Gáspár et al. (2009). All but one of our 24 μm excess candidates have spectral type F or later (based on their $V - K$ colors and fitted SEDs). We detect only one star earlier than F0 with 24 μm excess in NGC 2451A and none in NGC 2451B.

Our excess fractions among solar-type stars are $35\% \pm 12\%$ (5/15) in NGC 2451A and $39\% \pm 12\%$ (6/16) for NGC 2451 B, and for early-type stars are $29\% \pm 17\%$ (1/5) and $20\% \pm 20\%$ (0/3) for NGC 2451A and B, respectively.

5. DISCUSSION

5.1. Excess Fractions

Our results for excess fraction in the solar-type stars of NGC 2451B are roughly consistent with other clusters with similar ages such as IC 2391 (50 Myr—31%; Siegler et al. 2007) or NGC 2547 (35 Myr—40%; Gorlova et al. 2007). In the case of NGC 2451A, our excess fraction is significantly larger than that of M47 (80 Myr—6%; Gorlova et al. 2004) which

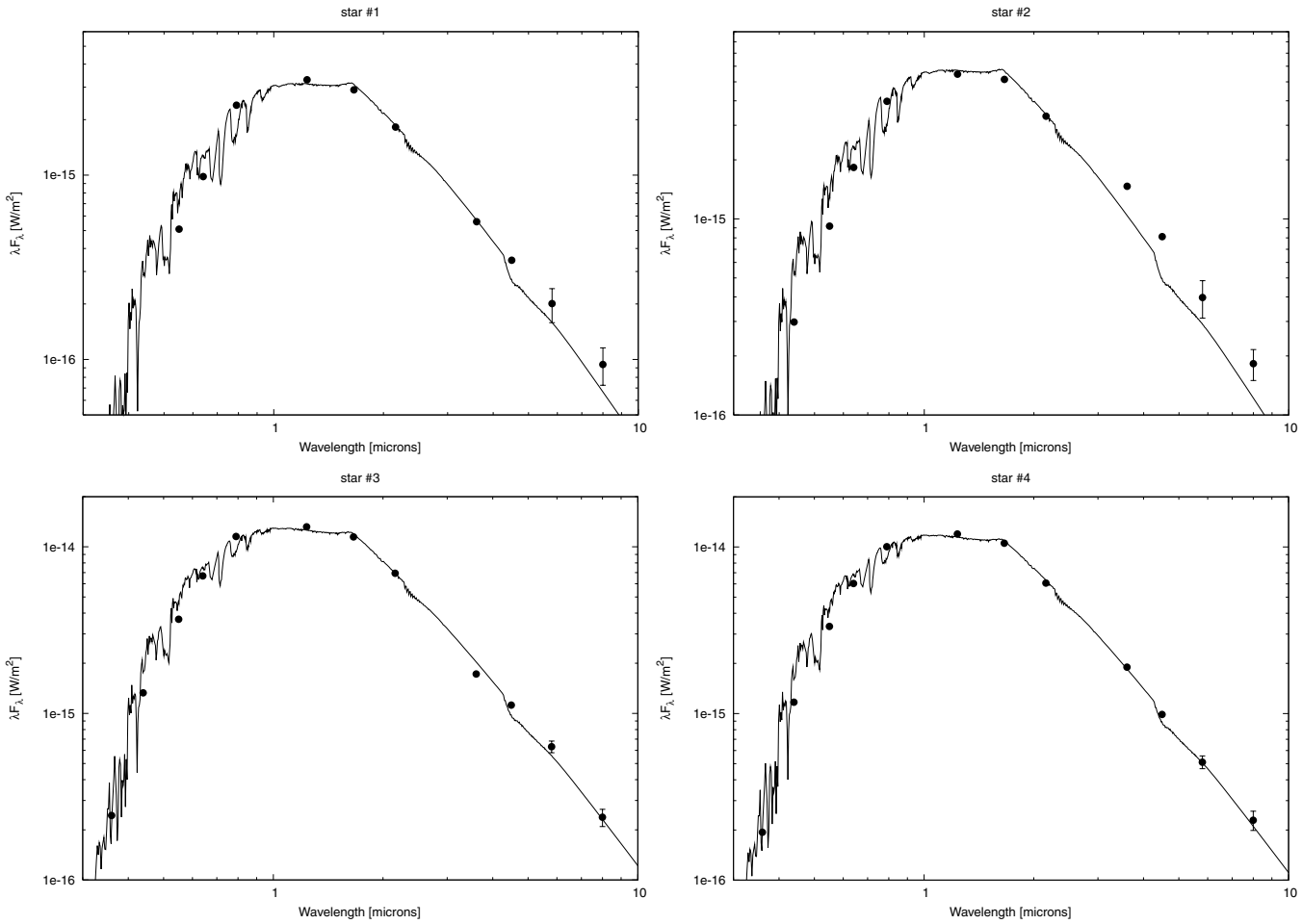

Figure 10. SEDs of the 8 μm excess candidates together with the fitted Kurucz atmospheric models. Error bars at 5.8 and 8.0 μm show the 3σ photometric errors.

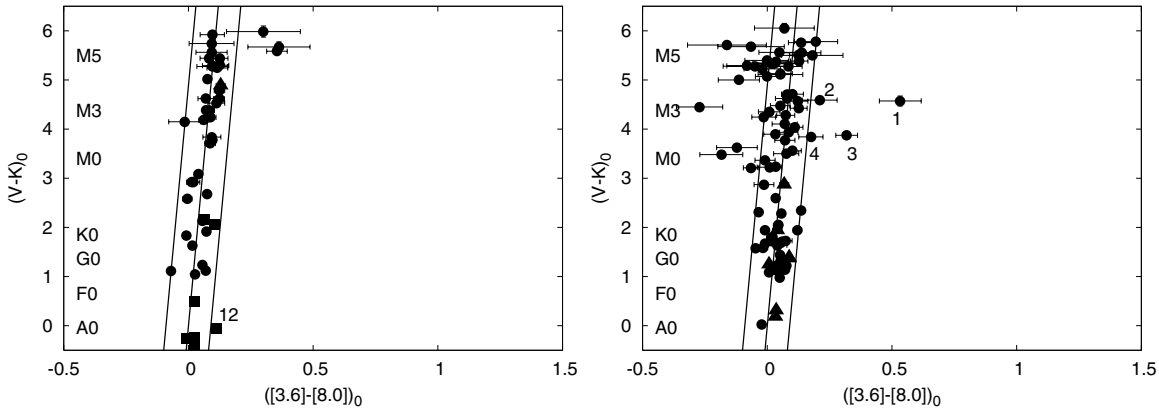

Figure 11. Same as Figure 7 but for $V - K$ vs. [3.6]–[8.0].

might indicate that the age of NGC 2451A is closer to 50 Myr rather than 80 Myr. However, the study of M47 has a higher threshold for detection of excesses, which might also account for the lower fraction.

For the early-type stars our results are in agreement with those of Siegler et al. (2007) and Su et al. (2006) who found a very low excess fraction (about 10% and 14% for IC2391 (50 Myr) and IC2602 (30 Myr), respectively).

Figure 15 shows the disk fractions as a function of age (similar to Figure 9 of Gáspár et al. 2009; left panel: early-type stars; right panel: late-type stars). Open circles show the data from Tables 4 and 6 of Gáspár et al. (2009), while filled squares designate the two new datapoints from our study. We note that for stars younger than 10 Myr the excess not necessarily indicates the presence of debris but primordial dust left over from the star formation process as pointed out by Rhee et al. (2007), so the first three points in the figure might overestimate the debris disk fraction. An interesting feature of the figures is that there is a dip in the fraction of debris disks in the age range of 30–80 Myr. Outside this range the decay seems to be monotonic. Our two clusters slightly deviate from the main trend in the late-type stars also but in a different direction. They are both situated above the main

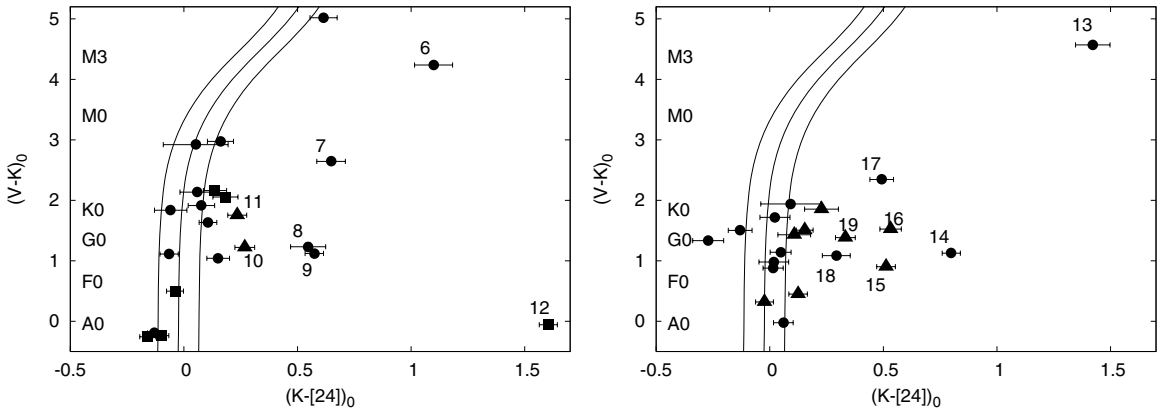

Figure 12. Same as Figure 7 but for $V - K$ vs. K-[24]. The solid lines represent the trendline (see the text) and its 3σ limits.

Table 7
Measured and Predicted Photospheric $(K\text{-}[24])_0$ Colors of Cluster Members with 24 μm Excesses

ID	R.A. (J2000)	Decl. (J2000)	$(K\text{-}[24])_0$ (mag)	$\sigma((K\text{-}[24])_0)$ (mag)	$(K\text{-}[24])_0^{\rm phot}$ (mag)	Significance of Excess
			NGC 2451A			
6	116.04942	−37.73994	1.099	0.084	0.271	9σ
7	116.74747	−38.37820	0.648	0.063	0.023	9σ
8	116.31223	−38.19624	0.547	0.077	−0.018	7σ
9	116.23017	−38.07956	0.574	0.041	−0.019	12σ
10	116.53718	−37.39910	0.268	0.043	−0.018	5σ
11	116.10025	−38.59977	0.235	0.042	−0.011	5σ
12	116.18701	−38.05376	1.604	0.040	−0.024	33σ
			NGC 2451B			
13	116.67488	−37.98390	1.422	0.076	0.353	13σ
14	115.95562	−37.89574	0.799	0.040	−0.022	17σ
15	116.21267	−37.66869	0.496	0.041	−0.023	11σ
16	116.50776	−38.00752	0.516	0.047	−0.022	10σ
17	116.44107	−37.89720	0.493	0.052	−0.010	9σ
18	116.74249	−37.63916	0.293	0.061	−0.024	5σ
19	116.36051	−38.19643	0.317	0.043	−0.025	7σ

locus of stars along with some other clusters of similar age. Incompleteness might account for the discrepancy. However, even if we remove the faintest stars (17 in Figure 12) in NGC 2451B and the three faintest ones (7 and the two photospheric sources around $V - K \sim 3$ in Figure 12, left panel) in NGC 2451A, the excess fractions ($35\% \pm 12\%$ and $36\% \pm 13\%$ for NGC 2451A and B, respectively) are still slightly above the main locus.

Unfortunately, low number statistics might reduce the reliability of these results. To check whether they are statistically significant we binned the cluster data of Gáspár et al. (2009) supplemented with our two clusters into five equal logarithmic age bins 3–10 Myr, 10–31.6 Myr, 31.6–100 Myr, 100–316 Myr, and 316–1000 Myr. We show the result of the binning in Figure 16 (left panel: early-type stars; right panel: late-type stars). There is a hint of a drop (about 1σ) in the excess fraction of early-type stars in the 31.6–100 Myr range then, a rise and another drop after 316 Myr. For the late-type stars, a small bump breaks the continuous decay with about the same significance as the dip in the early-type sample. More detailed and very accurate membership study of the clusters in this age range is necessary to decide whether this behavior can be attributed solely to statistical fluctuation.

5.2. Stars with Large Excesses

Among all stars in NGC 2451A/B showing excess at 24 μm, 12 (HD 62938) has by far the largest; K-[24] = 1.6 corresponding to an excess ratio (R) more than 4 meaning that the 24 μm flux density is more than four times larger than the expected photospheric flux level. The MIPS data place a 2σ upper limit of 63 mJy on the flux density at 70 μm, requiring a color temperature between 24 and 70 μm $\geqslant$95 K. To put this star into context with other results, we performed a literature search for main-sequence stars older than 20 Myr with similarly large or larger excess. We found nine stars with excess ratios larger than 4 at 24 μm. We also included two famous somewhat younger large excess stars HD39060 (β Pic) and HD181296 (η Tel) for comparison. They are listed in Table 8. The excess of HD21362, a B6 star, is due to free–free emission, so we rejected this star from our final sample.

Figure 17 shows the excess versus age diagram for our sample of 10 stars together with the sample of Rieke et al. (2005). We express the excess in $2.5 \times \log(R)$ so we can compare the Rieke et al. (2005) data with other publications where the excess is expressed in K-[24] mag. All but three of the stars with large excesses fall within the envelope of the decay trend of Rieke et al. (2005). The normalization of this envelope is somewhat

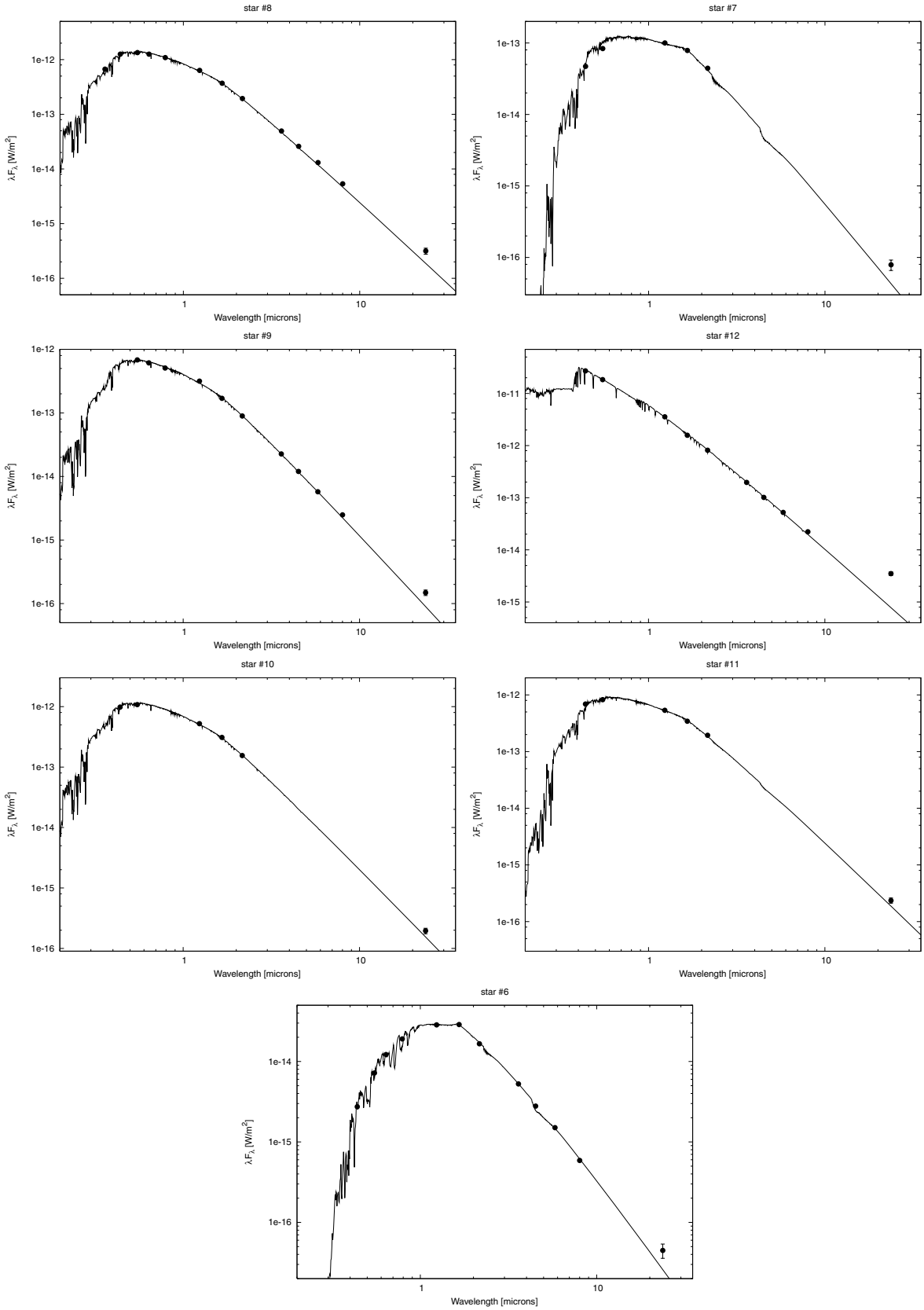

Figure 13. SEDs of the 24 μm excess candidates in NGC 2451A together with the fitted Kurucz atmospheric models. The error bars represent the 3σ photometric errors.

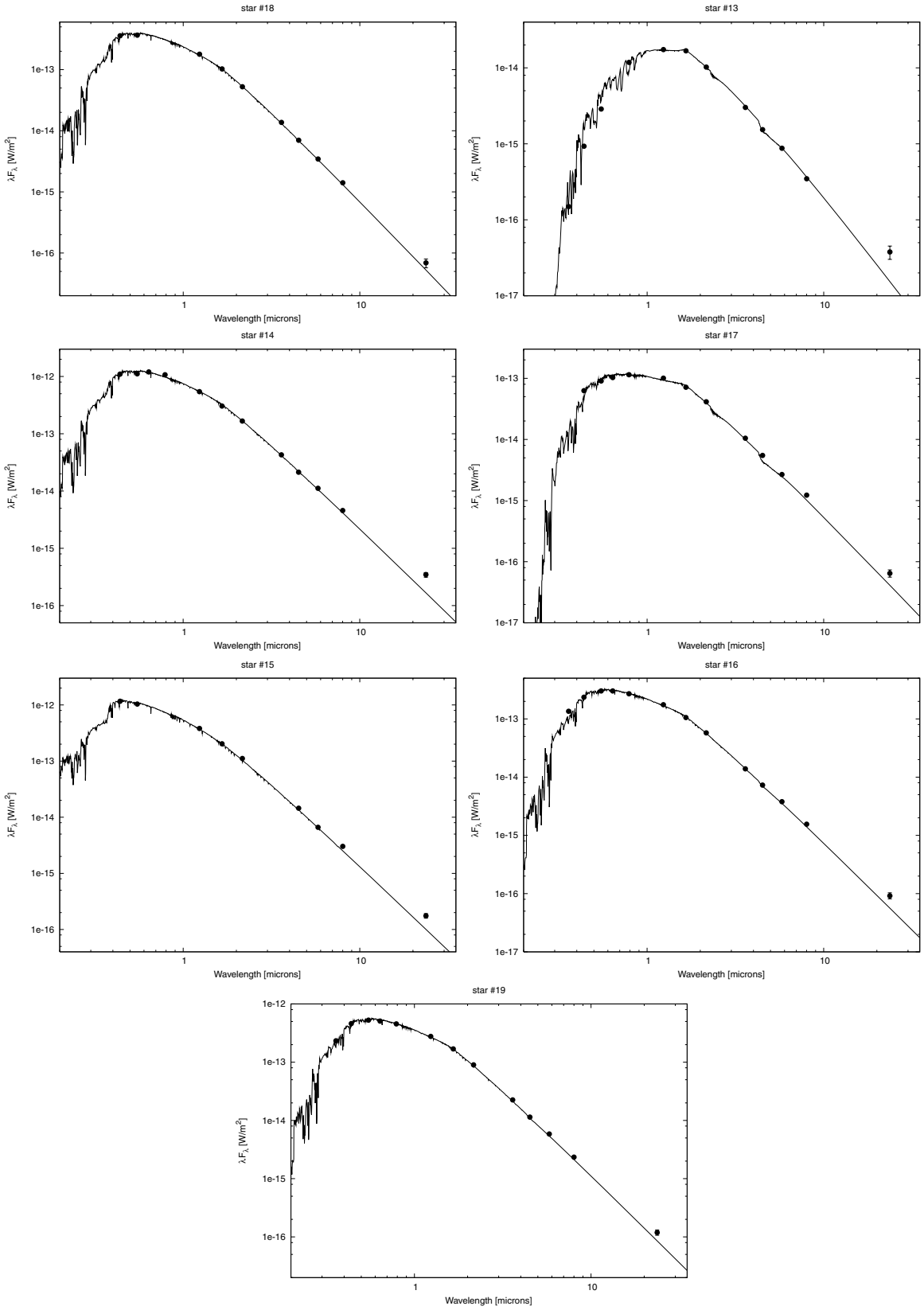

Figure 14. SEDs of the 24 μm excess candidates in NGC 2451B together with the fitted Kurucz atmospheric models. The error bars represent the 3σ photometric errors.

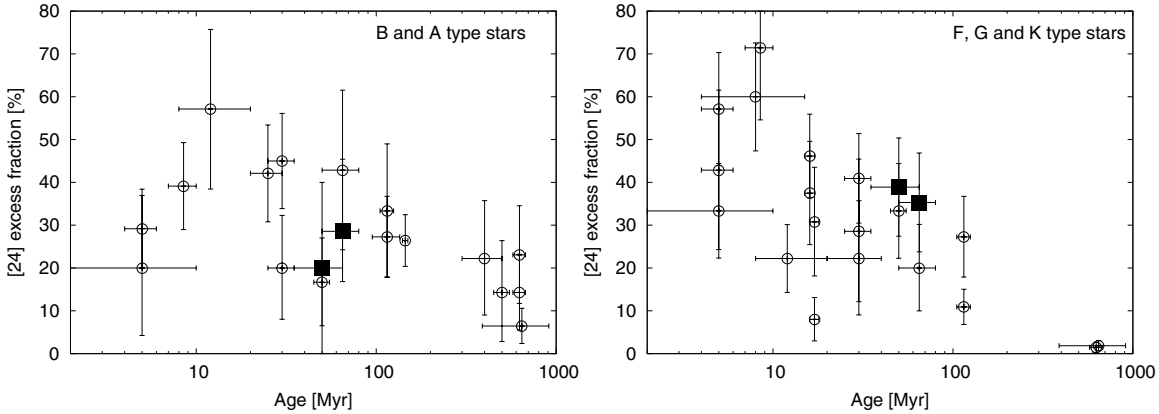

Figure 15. Fraction of stars with 24 μm excess vs. age in open clusters. Left panel: early-type stars. Right panel: solar-type stars. Open circles: data from Gáspár et al. (2009); filled squares: NGC 2451A and B.

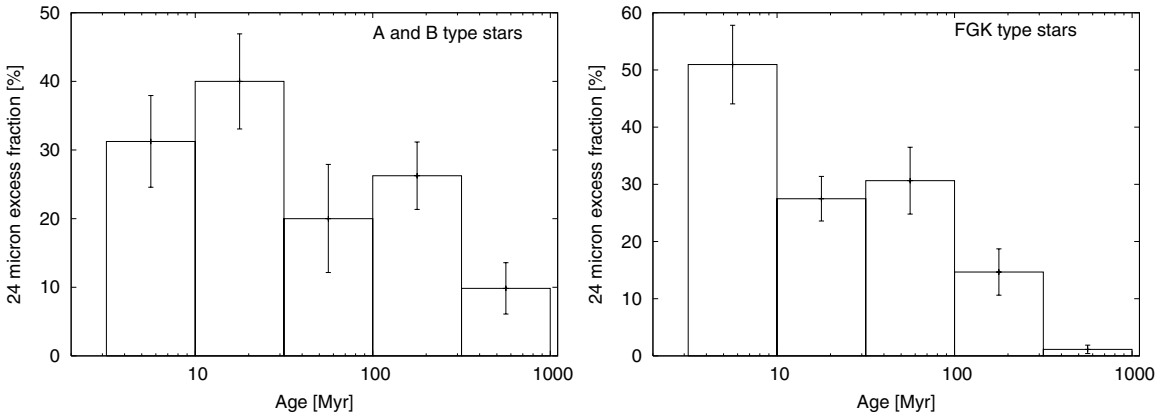

Figure 16. Binned excess fractions of open clusters vs. age. Left panel: early-type stars. Right panel: solar-type stars.

Table 8
Stars with Large 24 μm Excess

Name	SpT	Age	Excess Ref.	Age Ref.
HD21362[a]	B6Vn	80 Myr	Rieke et al. (2005)	Song et al. (2001)
HD39060	A5V	12 Myr	Rieke et al. (2005)	Ortega et al. (2002, 2004)
HD109573	A0V	10–20 Myr	Rieke et al. (2005)	Zuckerman & Song (2004a)
NSV17775[b]	A1V	25 Myr	Young et al. (2004)	Jeffries & Oliveira (2005)
NGC 2547/id8	G7V	35 Myr	Gorlova et al. (2007)	Jeffries & Oliveira (2005)
NGC 2547/id7	M	35 Myr	Gorlova et al. (2007)	Jeffries & Oliveira (2005)
P1121	F9V	80 Myr	Gorlova et al. (2004)	Rojo Arellano et al. (1997)
BD+20 307	G0	2 Gyr	Song et al. (2005)	Song et al. (2005)
HD23514	F6	120 Myr	Rhee et al. (2008)	Rhee et al. (2008)
HD181296	A0V	12 Myr	Su et al. (2006)	Zuckerman & Song (2004b)
HD62938 (12)	A0V	50–80 Myr	This work	Platais et al. (2001)

Notes.
[a] Excess comes from free–free emission.
[b] Incorrectly listed as a Cataclysmic Variable Star in SIMBAD.

arbitrary so no distinction should be made between stars just above or just below it. Two exceptions, P1121 of Gorlova et al. (2004) and HD23514 of Rhee et al. (2008), are young. The third one BD+20 307 (Song et al. 2005) is very old (about 2 Gyr; Zuckerman et al. 2008). The excesses of these stars are much higher than would be predicted based on their ages. Another two stars that are older than 30 Myr are borderline cases close to the upper envelope of the decay trend. One of them is a G7 star (ID8 in NGC 2547; Gorlova et al. 2007) the other is an M star in the same cluster (ID7). We retain these two stars as candidate extreme excess stars.

Although these stars were identified only on the basis of their large excesses at 24 μm, they have a number of unique characteristics in comparison with other debris disks. For example, without full spectral energy distributions we cannot compute the fractional luminosities, L_d/L_*, but we can put lower limits on this parameter. As an illustration, we assume a star represented by a 6000 K blackbody and a blackbodylike excess 10 times the stellar output at 24 μm. The minimum fractional luminosity is then 2×10^{-3} at an excess temperature of between 150 and 160 K. Seven of the 10 large excess stars are at this level or above. The minimum fractional luminosity

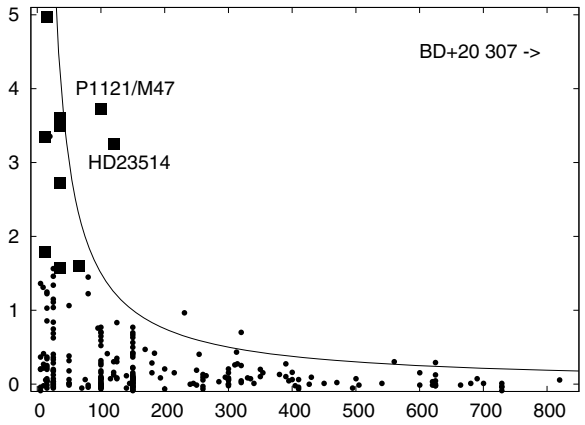

Figure 17. 24 μm excess vs. age. Squares: stars with large excess from Table 8; dots: stars from Rieke et al. (2005); solid line: the normal decay trend from IR excesses.

for the remaining three large excess sources is $\geqslant 2 \times 10^{-4}$. For comparison, debris disks typically have fractional luminosities below 10^{-4} (Moór et al. 2006). In addition, many of these systems are known to have strong spectral features in the mid-IR, establishing that their emission there is dominated by warm, very finely divided dust (β Pic, Chen et al. 2007; NGC 2547 ID8 and P1121, N. Gorlova et al. 2010, in preparation; BD +20 307, Song et al. 2005; HD 23514, Rhee et al. 2008).

These latter sources represent extreme examples of debris disks containing warm dust. Additional examples of systems with warm dust include Fomalhaut (Stapelfeldt et al. 2004); β Leo (Akeson et al. 2009, our unpublished observations); η Tel (Smith et al. 2009); η Corvi (Smith et al. 2008); HR 4796A (Wahhaj et al. 2005); ϵ Eri (Backman et al. 2009); HD 113766 (Lisse et al. 2008); HD 69830 (Beichman et al. 2005); and ζ Lep (Moerchen et al. 2007). Morales et al. (2009) report 28 additional systems with dust at $T \geqslant 180$ K and that dominates the disk emission at 24 μm. It is therefore plausible that many of the other large excess systems have substantial emission by warm dust.

Although many of the large-excess stars are roughly of solar type, even in this case they are relatively uncommon. In particular, for the 30–130 Myr age range, Table 8 shows there are only three solarlike extreme excess stars. They are drawn from a parent population of all the stars observed within this age range and with spectral types between mid-F (F4) and mid-K (K4), a total of about 250 (from M47, Gorlova et al. 2004; the Pleiades, Stauffer et al. (2005), Gorlova et al. 2006, and our unpublished work; IC 2391, Siegler et al. 2007; NGC 2547, Gorlova et al. 2007; the FEPS sample, Meyer et al. 2008; and NGC 2451A and B, this work). That is, the incidence of extreme excess systems among solar-like stars in the 30–130 Myr age range is only about 1%.

The 30–130 Myr age range insures that these extreme excesses are unlikely to originate in the wave of oligarth planet building that peaks around 10–15 Myr (e.g., Currie et al. 2008 and references therein). There are alternative possibilities for generating them, however. One is collisions between large bodies, similar to the collision that led to the formation of the Moon (Rhee et al. 2008). It is thought that about three moon masses of material were thrown into orbit around the Sun in the impact that formed our Moon (Canup 2004). The rapid injection of such a large mass would produce a signature roughly in agreement with the observations of these large-excess objects (N. Gorlova et al. 2010, in preparation). A rough e-folding time of 2 million years for the dissipation of this mass can be estimated from the calculations of Grogan et al. (2001). In addition, a process that results in very vigorous gravitational stirring of a dense asteroid belt (e.g., through gravitationally resonant orbits of massive planets, Gomes et al. 2005) is also a candidate to produce huge IR excesses.

Although Table 8 contains several early-type stars older than 20 Myr and with large excesses, none of them is above the decay trend of normal debris disk stars. In fact, as Table 8 emphasizes, all the large-excess early-type stars are relatively young and may just still be in the decay of their initial peak debris output. The placement of the trend line is rather arbitrary. Nevertheless, we have considered why no very large excesses are found for older early-type stars. We calculated what mass would be needed to cause an excess about four times above the stellar photosphere at 24 μm in an A star. We used only grains larger than 6.3 μm, because radiation pressure will eject small grains from the system, with terminal velocity $v = \frac{2GM_\star}{r_{\rm init}}(\beta - \frac{1}{2})^{\frac{1}{2}}$, where $M_\star$ is the mass of the central star, $r_{\rm init}$ is the radius of the initial orbit of the grain, and β is the ratio of forces from radiation pressure and gravity. Dominik & Decin (2003) showed that the orbiting grains normally dominate the visibility of the debris disk over the blown-out grains. To get the total mass needed to cause the required 24 μm excess we first assumed that all the flux comes from the smallest grains then we calculated the total surface area of these grains. Using the surface area and the $N(a) \sim a^{-3.5}$ grain size distribution, we were able to determine the scaling constant using the following equation:

$$\int_{a_{\rm min}}^{a_{\rm max}} 4\pi \frac{a^2}{4} c a^{-3.5} da = N_{a_{\rm min}} 4\pi \frac{a_{\rm min}^2}{4}, \quad (6)$$

where $a_{\rm min}$ is the diameter of the smallest grain remaining in the system and $a_{\rm max}$ is a nominal maximum parent planetesimal size (100 m). Using the scaling constant, we can calculate the total mass by integrating $\frac{4}{3}\pi a^3 \rho c a^{-3.5}$ from $a_{\rm min}$ to $a_{\rm max}$. We found that the total mass needed to produce the excess is on the order of a couple of Moon masses. The same calculation for G-type stars with $a_{\rm min} = 0.01$ μm leads to 2 orders of magnitude less mass ($\sim 10^{-2}$ $M_{\rm Moon}$).

In the case of A stars, radiation pressure clears the small grains from the disk in a few hundred years, while these grains remain around the G-star for a few times 10^4 years (Chen et al. 2005). To quantify the effects of this difference, we also calculated the scaling factor and the total mass neglecting the effect of blowout for the A star and integrating over the entire size range from 10^{-2} μm to 100 m. We found that in this case we would need more than 25 times less material for producing the same level of excess around the A star. In this hypothetical case, the masses needed for A- and G-type stars are the same order of magnitude. This implies that their ability to eject grains very efficiently through photon pressure plays a large role in the absence of extreme excess around older early-type stars. Those small grains carry a large surface area (relative to their mass) which would make the excess more easily detectable. A corollary is that large grain production rates around early-type stars will be indicated by large flows of small grains out of the system driven by photon pressure. Possible examples include Vega (Su et al. 2005) and HR8799 (K. Y. L. Su et al. 2010, in preparation).

6. CONCLUSIONS

We present optical and *Spitzer*/IRAC-MIPS photometry and medium-resolution spectroscopy of the central 0.75 deg^2 region of NGC 2451A and B. Using radial velocity data and optical/near-IR CMDs, we selected 61 members of NGC 2451A and 131 members of NGC 2451B. We found one object in NGC 2451B and none in NGC 2451A with excess at 8 μm. We conclude that 8 μm excesses at the ages of these clusters are probably associated with an isolated event that disturbs the distribution of planetesimals to yield a sequence of collisional cascades producing dust.

We find one object with 24 μm excess among the early-type stars of NGC 2451B and none in NGC 2451A. For the solar-type stars, we found five out of 15 stars with excess in NGC 2451A and seven out of 16 for NGC 2451B. In general, these results agree with excess fractions reported in the literature.

We used the data presented in Gáspár et al. (2009) supplemented with our new datapoints to plot the excess fraction versus age, and found that the excess fraction unexpectedly drops in the range of 30–80 Myr for early-type stars, while it slightly rises in the same age for late-type stars. We tested our findings by binning the cluster data of Gáspár et al. (2009) into equal logarithmic age bins. The results are consistent with some structure but also indicate that the fluctuations may be statistical in nature.

We summarize the detections to date of large debris-disk 24 μm excesses. There are only five extreme cases, with fractional luminosities $\geqslant 2 \times 10^{-3}$. We did not find extreme excesses around older early-type stars, excesses that would indicate a catastrophic collision between forming planetesimals. We found that blowout of the small grains probably plays a very important role in the lack of detections.

We thank the anonymous referee for comments and suggestions that greatly improved the manuscript. This work is based on observations made with the *Spitzer Space Telescope*, which is operated by the Jet Propulsion Laboratory, California Institute of Technology, under NASA contract 1407. Support for this work was provided by NASA through contract 1255094, issued by JPL/Caltech. Z.B. also received support from Hungarian OTKA Grants T049082 and K76816. L.L.K. has been supported by the Anglo-Australian Observatory and the Australian Research Council.

REFERENCES

Akeson, R. L., et al. 2009, ApJ, 691, 1896
Andretta, V., Busà, I., Gomez, M. T., & Terranegra, L. 2005, A&A, 430, 669
Backman, D., et al. 2009, ApJ, 690, 1522
Beichman, C. A., et al. 2005, ApJ, 626, 1061
Canup, R. M. 2004, ARA&A, 42, 441
Chen, C. H., et al. 2005, ApJ, 634, 1372
Chen, C. H., et al. 2007, ApJ, 666, 466
Currie, T., Kenyon, S. J., Balog, Z., Rieke, G., Bragg, A., & Bromley, B. 2008, ApJ, 672, 558
Dominik, C., & Decin, G. 2003, ApJ, 598, 626
Fazio, G. G., et al. 2004, ApJS, 154, 10
Gáspár, A., Rieke, G. H., Su, K. Y. L., Balog, Z., Trilling, D., Muzerolle, J., & Apai, D. 2009, ApJ, in press (arXiv:0903.4193)
Gomes, R., Levison, H. F., Tsiganis, K., & Morbidelli, A. 2005, Nature, 435, 466
Gordon, K. D., et al. 2005, PASP, 117, 503
Gorlova, N., Balog, Z., Rieke, G. H., Muzerolle, J., Su, K. Y. L., Ivanov, V. D., & Young, E. T. 2007, ApJ, 670, 516
Gorlova, N., Rieke, G. H., Muzerolle, J., Stauffer, J. R., Siegler, N., Young, E. T., & Stansberry, J. A. 2006, ApJ, 649, 1028
Gorlova, N., et al. 2004, ApJS, 154, 448
Grogan, K., Dermott, S. F., & Durda, D. D. 2001, Icarus, 152, 251
Gutermuth, R. A., Megeath, S. T., Muzerolle, J., Allen, L. E., Pipher, J. L., Myers, P. C., & Fazio, G. G. 2004, ApJS, 154, 374
Gutermuth, R. A., et al. 2008, ApJ, 674, 336
Hünsch, M., Randich, S., Hempel, M., Weidner, C., & Schmitt, J. H. M. M. 2004, A&A, 418, 539
Hünsch, M., Weidner, C., & Schmitt, J. H. M. M. 2003, A&A, 402, 571
Jeffries, R. D., & Oliveira, J. M. 2005, MNRAS, 358, 13
Kharchenko, N. V., Piskunov, A. E., Röser, S., Schilbach, E., & Scholz, R.-D. 2005, A&A, 438, 1163
Kiss, L. L., Szabó, G. M., Balog, Z., Parker, Q. A., & Frew, D. J. 2008, MNRAS, 391, 399
Kiss, L. L., Székely, P., Bedding, T. R., Bakos, G. Á., & Lewis, G. F. 2007, ApJ, 659, L129
Landolt, A. U. 1992, AJ, 104, 340
Lisse, C. M., Chen, C. H., Wyatt, M. C., & Morlok, A. 2008, ApJ, 673, 1106
Meyer, M. R., et al. 2008, ApJ, 673, L181
Moerchen, M. M., Telesco, C. M., Packham, C., & Kehoe, T. J. J. 2007, ApJ, 655, L109
Moór, A., Ábrahám, P., Derekas, A., Kiss, C., Kiss, L. L., Apai, D., Grady, C., & Henning, T. 2006, ApJ, 644, 525
Morales, F. Y., et al. 2009, ApJ, in press
Munari, U., Sordo, R., Castelli, F., & Zwitter, T. 2005, A&A, 442, 1127
Ortega, V. G., de la Reza, R., Jilinski, E., & Bazzanella, B. 2002, ApJ, 575, L75
Ortega, V. G., de la Reza, R., Jilinski, E., & Bazzanella, B. 2004, ApJ, 609, 243
Platais, I., Kozhurina-Platais, V., Barnes, S., Girard, T. M., Demarque, P., van Altena, W. F., Deliyannis, C. P., & Horch, E. 2001, AJ, 122, 1486
Rhee, J. H., Song, I., & Zuckerman, B. 2007, ApJ, 671, 616
Rhee, J. H., Song, I., & Zuckerman, B. 2008, ApJ, 675, 777
Rieke, G. H., et al. 2004, ApJS, 154, 25
Rieke, G. H., et al. 2005, ApJ, 620, 1010
Rojo Arellano, E., Pena, J. H., & Gonzalez, D. 1997, A&AS, 123, 25
Siegler, N., Muzerolle, J., Young, E. T., Rieke, G. H., Mamajek, E. E., Trilling, D. E., Gorlova, N., & Su, K. Y. L. 2007, ApJ, 654, 580
Siess, L., Dufour, E., & Forestini, M. 2000, A&A, 358, 593
Smith, R., Churcher, L. J., Wyatt, M. C., Moerchen, M. M., & Telesco, C. M. 2009, A&A, 493, 299
Smith, R., Wyatt, M. C., & Dent, W. R. F. 2008, A&A, 485, 897
Song, I., Caillault, J.-P., Barrado y Navascués, D., & Stauffer, J. R. 2001, ApJ, 546, 352
Song, I., Zuckerman, B., Weinberger, A. J., & Becklin, E. E. 2005, Nature, 436, 363
Stapelfeldt, K. R., et al. 2004, ApJS, 154, 458
Stauffer, J. R., et al. 2005, AJ, 130, 1834
Steinmetz, M., et al. 2006, AJ, 132, 1645
Su, K. Y. L., et al. 2005, ApJ, 628, 487
Su, K. Y. L., et al. 2006, ApJ, 653, 675
Touboul, M., Kleine, T., Bourdon, B., Palme, H., & Wieler, R. 2007, Nature, 450, 1206
Wahhaj, Z., Koerner, D. W., Backman, D. E., Werner, M. W., Serabyn, E., Ressler, M. E., & Lis, D. C. 2005, ApJ, 618, 385
Young, E. T., et al. 2004, ApJS, 154, 428
Zuckerman, B., Fekel, F. C., Williamson, M. H., Henry, G. W., & Muno, M. P. 2008, ApJ, 688, 1345
Zuckerman, B., & Song, I. 2004a, ARA&A, 42, 685
Zuckerman, B., & Song, I. 2004b, ApJ, 603, 738
Zwitter, T., et al. 2008, AJ, 136, 421